THESIS FOR THE DEGREE OF DOCTOR OF PHILOSOPHY IN SOLID AND STRUCTURAL MECHANICS

Numerical investigations of rolling contact fatigue crack growth in a rail head

MOHAMMAD SALAHI NEZHAD

Department of Industrial and Materials Science
Division of Material and Computational Mechanics
CHALMERS UNIVERSITY OF TECHNOLOGY

Göteborg, Sweden 2024

Numerical investigations of rolling contact fatigue crack growth in a rail head
MOHAMMAD SALAHI NEZHAD
ISBN 978-91-8103-074-7

Doktorsavhandlingar vid Chalmers tekniska högskola
Ny serie nr. 5532
ISSN 0346-718X
Department of Industrial and Materials Science
Division of Material and Computational Mechanics
Chalmers University of Technology
SE-412 96 Göteborg
Sweden
Telephone: +46 (0)31-772 1000

Cover:
Cracks (head checks) in a rail. Photo [Anders Ekberg] (left), and illustration of modelled cracks and contact load (right).

Chalmers Reproservice
Göteborg, Sweden 2024

Numerical investigations of rolling contact fatigue crack growth in a rail head

MOHAMMAD SALAHI NEZHAD
Department of Industrial and Materials Science
Division of Material and Computational Mechanics
Chalmers University of Technology

Abstract

Rolling Contact Fatigue (RCF) cracks in railway rails are critical due to their impact on safety and maintenance costs. A rail break can be the ultimate consequence of progressive crack growth. Understanding influential mechanisms involved in RCF initiation and propagation is essential for developing effective inspection, maintenance, and replacement strategies. Despite extensive research on understanding mechanisms, and predicting RCF crack growth, there are still open questions, particularly regarding the direction and rate of RCF crack growth. This is due to the complex non-proportional and compressive loading from wheel–rail contact in combination with rail bending and thermal loads.

This thesis aims to develop and employ a numerical framework for predicting directions and rates for RCF crack growth in railway rails under operational loading. A numerical procedure for simulating a propagating crack in 2D is developed. The finite element model features an inclined surface-breaking crack subjected to wheel–rail contact load, rail bending, and temperature drop as isolated scenarios and in combinations. The effective crack propagation direction is predicted based on an accumulative vector crack tip displacement criterion. The influence of crack face friction and crack growth rate predictions are added to the numerical framework. It is observed that frictional cracks tend to go deeper into the rail under a pure contact load and under a combination of bending and contact loads, while friction has a moderate influence on crack paths under combined tensile thermal and contact loads. Furthermore, friction reduces crack growth rates.

The numerical framework for a frictionless stationary crack is extended to the 3D case of a semi-circular gauge corner crack embedded in a 60E1 rail. Results are evaluated at points along the crack front. The influence of crack size and inclination, magnitude and position of the contact load, wheel–rail tractive forces, rail bending with different track support conditions, and varying thermal loads is studied. Rail bending and tensile thermal loads are found to promote downward growth compared to pure contact load cases. The location of the contact load significantly influences predicted growth rates while the influence of a tractive force decreases (rapidly) with depth. Rail lives computed from the integration of predicted growth rates are comparable to growth rates found in field investigations.

Keywords: Rolling contact fatigue, Crack growth direction, Crack growth rate, Vector crack tip displacement, Paris law, Crack face friction, Finite element analysis, Rail deterioration.

To my beloved wife, Maryam.

Preface

The work in this thesis was carried out between September 2019 and July 2024 at the Department of Industrial and Materials Science at Chalmers University of Technology within the research project MU38 "Growth of rolling contact fatigue cracks". The study is part of the ongoing activities within the center of excellence CHARMEC – Chalmers Railway Mechanics (`www.chalmers.se/charmec`). Parts of the project have been funded by the European Union's Horizon 2020 research and innovation programme in the Shift2Rail projects In2Track2 under grant agreement No. 826255 and In2Track3 under grant agreement No. 101012456. Funding has also been received from the Horizon Europe research and innovation programme in Europe Rail project IAM4RAIL under grant agreement No. 101101966. Some of the computations were performed on resources provided by Chalmers e-Commons at Chalmers.

Acknowledgements

First and foremost, I would like to sincerely thank my supervisors, Professor Fredrik Larsson, Professor Elena Kabo, and Professor Anders Ekberg for their endless support, great patience and encouragement, and excellent guidance. I am truly happy to have had the chance to work with you all and have surely learned a lot through this journey. Special thanks go to Dr. Dimosthenis Floros, who gave me a lot of help and support during the early stage of the project.

I would also like to thank all my colleagues and friends at the Division of Material and Computational Mechanics and the Division of Dynamics for creating a joyful work environment. These years would not be as fun without you!

Finally, I want to express my heartfelt gratitude to my family for their love and support. Last but definitely not least, my highest appreciation would go to my beloved wife Maryam, for her understanding, patience, and endless support.

Gothenburg, July 2024
Mohammad Salahi Nezhad

Thesis

This thesis consists of an extended summary and the following appended papers:

Paper A M. Salahi Nezhad, D. Floros, F. Larsson, E. Kabo, A. Ekberg. Numerical predictions of crack growth direction in a railhead under contact, bending and thermal loads. *Engineering Fracture Mechanics* **261** (2022), 108218. DOI: 10.1016/j.engfracmech.2021.108218

Paper B M. Salahi Nezhad, F. Larsson, E. Kabo, A. Ekberg. Numerical prediction of railhead rolling contact fatigue crack growth. *Wear* **530–531** (2023), 205003. DOI: 10.1016/j.wear.2023.205003

Paper C M. Salahi Nezhad, F. Larsson, E. Kabo, A. Ekberg. Finite element analyses of rail head cracks: Predicting direction and rate of rolling contact fatigue crack growth. *Submitted for international publication.*

Paper D M. Salahi Nezhad, E. Kabo, A. Ekberg, F. Larsson. Rolling contact fatigue crack propagation in rails – numerical investigation on consequences of operational load variations. *To be submitted for international publication.*

The appended papers were prepared in collaboration with the co-authors. The author of this thesis was responsible for the major part of the work, that is, took part in planning the papers, developed the theoretical and computational framework, carried out numerical implementation and simulations, interpreted the results, and wrote major parts of the papers. In addition, the author was responsible for managing the submission and peer-review process for **Papers A–C**.

Other publication related to this thesis

The following publication is not included in this thesis due to an overlap in content:

M. Salahi Nezhad, F. Larsson, E. Kabo, A. Ekberg. Numerical prediction of rolling contact fatigue crack growth in a railhead. *Proceedings of the 12th International Conference on Contact Mechanics and Wear of Rail/Wheel Systems (CM 2022)*, Melbourne, Australia (2022), pp. 428–435.

Contents

Part I
Extended Summary

1 Introduction

1.1 Background and motivation

Railway transportation is generally a safe and efficient mode of transport with a low carbon footprint. A study from Sweden in 2008 shows that rail transports are about fifty to one hundred times safer than road transports [1]. On a global level in 2016, about 8% of passengers and 7% of freight movements were transported via railways while consuming less than 2% of transport energy [2]. The efficiency is related to the steel-to-steel wheel–rail contact, which gives a (relatively) low rolling resistance [3], and large load capacity. Also, railways have low CO_2 emissions per passenger-kilometer and tonne-kilometer [4].

Thanks to these advantages, demand for rail transportation has increased in recent decades and is expected to rise significantly until 2050 [2]. However, the amount of available tracks increases at a slower rate than the transport volumes due to expensive infrastructure. This means that the availability for inspections and maintenance is decreasing while the consequences of insufficient maintenance become larger and larger. The situation can be further aggravated by the limited possibility of rerouting railway traffic.

Following Hertzian contact theory [5], one consequence of having stiff contacting materials would be very high contact stresses between the contacting bodies [3]. The maximum contact pressure in the wheel–rail contact can exceed 1000 MPa [6]. Additional tractive forces are also acting in the wheel–rail interface, particularly in conjunction with braking, accelerating, and negotiating curves. Rolling Contact Fatigue (RCF) cracks are an inevitable consequence of such high stresses, see Fig. 1.1. These cracks are widespread and costly to mitigate, potentially leading to traffic disruptions and affecting the reliability and safety of the railways if not treated in time. The annual maintenance of RCF cracks can cost millions of euros, depending on the network, as indicated in [7, 8]. Therefore, the ability to understand and predict the behaviour of these cracks, allowing for optimisation of rail maintenance, would be of utmost interest to railway infrastructure managers.

RCF cracks can grow either downwards into the rail head or towards the rail surface. The former can cause rail breaks, which are obvious safety risks, while the latter can lead to spalling of the rail material. Modified contact conditions resulting from, e.g., spalling of the rail, can also change the dynamic response of the track. This may worsen the situation. In addition to the wheel–rail contact load with high compressive and shear

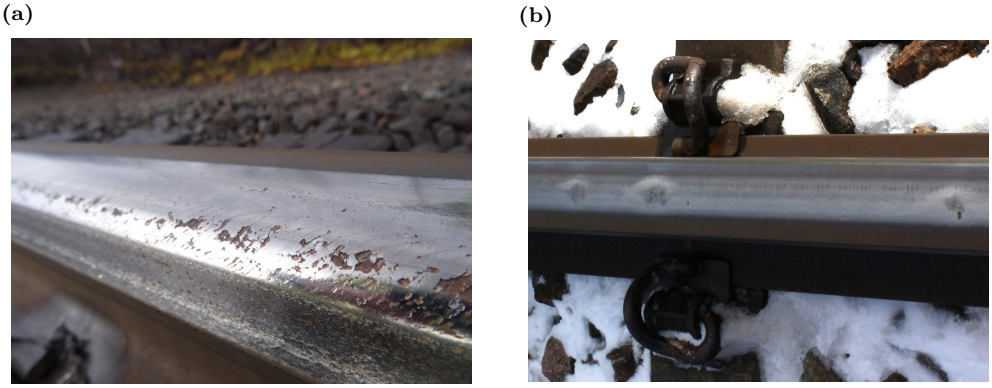

Figure 1.1: *RCF cracks in rails. (a) Head checks. (b) Squats. Photos: Anders Ekberg.*

components, other loads also affect the rails. Examples are rail bending, tensile thermal stresses in the continuously welded rails due to the restricted thermal contraction, and residual stresses due to welding and/or rail manufacturing. The resulting RCF cracks thus grow under a very complicated non-proportional mixed-mode and compressive loading, which makes the prediction of the development of RCF cracks much more complex than for 'plain' fatigue [1] cases [9]. Therefore, there are still many open questions, especially regarding RCF crack propagation in the zone near the rail surface.

Two of the most common types of RCF cracks in railways are head checks and squats [10]. Head checks generally appear at the gauge corner of the higher rail in curves as a series of inclined, tightly spaced surface cracks, see Fig. 1.1a. They are initiated by plastic strain accumulation due to frictional wheel–rail contact [11]. Squats typically occur on the running band of (near) tangent tracks as isolated depressions, see Fig. 1.1b. They are initiated mainly by rail surface defects such as indentations, martensite, and short-pitch corrugations, along with the resulting high-frequency dynamic forces [11]. Despite the differences, the adopted concept of crack propagation analysis for these RCF cracks is (to a large extent) identical in the literature.

In a crack propagation study, three general questions typically need to be addressed:

1. When is a crack (of a certain size and orientation) formed? (initiation)

2. In which direction does a crack tend to grow? (growth direction)

3. How fast does a crack propagate? (growth rate)

This thesis focuses on the crack growth direction and rate (second and third questions). Regarding crack *initiation* in rails, more information can be found in e.g., [12, 13].

[1] In 'plain' or 'classic' fatigue (as opposed to multiaxial fatigue), the cyclic loading is uniaxial.

1.2 Aim and scope of research

Having a deeper understanding of the behaviour of RCF cracks is crucial for optimising maintenance procedures. There are still significant uncertainties in predicting crack growth, particularly regarding the direction and rate of propagation. This study aims to improve the predictions of RCF crack growth in rails under operational loading scenarios. In particular, the goal is to investigate crack growth direction and rate for an existing (macroscopic) crack using Finite Element (FE) simulations in 2D and 3D primarily setting out from available tools in the literature and further improving these when needed. This leads to the following specific research objectives:

1. Develop a numerical framework in 2D and 3D for predicting crack growth directions and rates in a rail featuring an isolated surface-breaking inclined RCF crack under relevant operational load scenarios.
2. Investigate the influence of operational parameters to determine the influential ones.
3. Investigate the influence of model dimensions (2D and 3D) on predicted results.
4. Describe practical implications of the obtained results.

There are some restrictions on the conducted study in this thesis. Firstly, the process of crack initiation is not considered. Also, the rail material is assumed to be linearly elastic. Thereby, this research does not take into account the influence of existing anisotropy very close to the rail surface. Moreover, the influence of wear-off and residual stresses in the rail is not considered. In addition, the obtained results are based solely on macroscopic models, i.e., microstructural effects are not considered in this study. Finally, predictions of crack growth rates should be taken as qualitative since model parameters need to be further calibrated towards experimental data for more quantitative predictions.

1.3 Thesis outline

The remainder of this extended summary is structured as follows. Important topics regarding the prediction of rolling contact fatigue crack growth are presented in Chapter 2. The numerical framework employed in this thesis is introduced in Chapter 3. A brief summary of appended papers with some main results is given in Chapter 4. Finally, the main conclusions from the study with their practical implications, and some suggestions for future work are discussed in Chapter 5.

2 Prediction of rolling contact fatigue crack growth

2.1 Stress Intensity Factors

Linear Elastic Fracture Mechanics (LEFM) is the dominant theory for studying crack growth and fracture. The most important assumption in LEFM is that the material response can be modelled as linear elastic. This implies that only small-scale yielding at the tip of a macroscopic crack is allowed. Irwin in 1957 introduced a scalar parameter known as the 'Stress Intensity Factor (SIF)' to quantify the severity of the crack loading in the analytical solution of elasticity problems [14]. This parameter has since been widely used in LEFM.

SIFs are important parameters in LEFM as (almost) all desired quantities in the vicinity of a crack tip/front such as stress, energy and displacements can be described in terms of SIFs. As a result, there is a lot of effort in the literature to evaluate these parameters under various conditions using experimental, analytical, and numerical methods.

Available solutions in handbooks [15, 16, 17] are examples of analytical solutions. These methods can typically be used for idealized conditions (geometries and loadings), and are generally not very suitable for complex cases. For these applications, numerical methods are used to estimate SIFs and their evolution.

In computational fracture mechanics, the Boundary Element Method (BEM) and the Finite Element Method (FEM) are two common approaches for SIF evaluations. In this thesis, FEM is employed. An Overview of FEM approaches is given in e.g., [18]. A review of approaches based on BEM is described in [19]. A combination of numerical and analytical methods can also be used such as in hybrid and alternating methods described in [20].

A common approach to evaluate SIFs in LEFM analyses, particularly in commercial software, is by using the J-integral [21, 22]. However, the method is usually not the best option for RCF crack growth due to issues related to crack closure resulting from high compressive forces.

Another method for SIF evaluation is to use the displacement or stress fields in the vicinity of the crack tip (in the crack local coordinate system shown in Fig. 2.2) [23]. This approach is straightforward and can be adopted either directly with a very fine mesh around the crack or in combination with parameter estimation methods. As lower computational costs for 2D simulations can make using a dense mesh around the crack feasible, a direct displacement-based method can be used in 2D. However, mesh refinement in 3D models can substantially increase the computational cost. To have good accuracy in SIF computations with reasonably low computational cost, a displacement-based method employing a relatively fine mesh in combination with a least squares formulation is

developed in [24]. The method fits a low-order asymptotic displacement field ansatz to the displacement obtained from an analysis using FEM/eXtended Finite Element Method (XFEM)[1] over an integration domain defined around the desired point on the crack front. This method is particularly suitable for multiaxial load cases especially those with (large) shear and compressive loads, which is the case for the wheel–rail contact. This is achieved by considering three terms in the presumed ansatz: stress singularities, rigid body motion and uniform strain fields. Another advantage of the method is its simplicity and ease of implementation. Note however that caution must be taken when using the method near free surfaces due to the assumption of plane strain conditions in the employed displacement ansatz for the stress singularities term.

2.2 Crack modelling by use of FEM

Representation of cracks is one of the most difficult, and often time-consuming, aspects of numerical modelling of cracked bodies. In principle, the approaches in FE crack modelling can be divided into *discontinuous* methods, where there is a discontinuity in the displacement field along the crack, and *continuous* methods, where the displacement field is considered continuous along the crack. The former approaches are briefly discussed in the following as they are employed in this thesis.

Discontinuous, also known as *explicit* or *discrete*, crack modelling is the oldest approach in the field [25]. It started with employing a crack directly into the FE mesh with standard elements, i.e., having separate sets of nodes for the top and bottom surfaces of the crack. This method provides an accurate representation of the crack geometry. However, the quality of the mesh around the crack is of great importance. This often makes it cumbersome to generate a good quality FE mesh in the crack area, especially for complex crack geometries. Further, FE mesh needs to be regenerated for each crack growth increment in a crack propagation analysis [18].

A remedy is considering special elements close to the crack tip/front. The basic idea is to modify the position of the middle nodes of the elements to better capture the singularity close to the crack. These elements are often called singular elements and one of the most famous elements in this category is the quarter-point element [26, 27], where the middle node moves to the quarter-point in the direction of crack tip/front. Regarding crack propagation analyses, employing adaptive remeshing techniques can also improve the accuracy and efficiency of the simulations, see e.g., [28] for a review of these techniques for 3D fatigue crack growth modelling.

Another method, called the eXtended Finite Element Method (XFEM), was introduced in [29, 30] to facilitate the meshing process. In this method, the standard FE approximation for displacement field, $\mathbf{u}^{\mathrm{FE}}(\mathbf{x})$, is enriched with additional functions for the cracked elements [30]. As shown in Fig. 2.1 for a 2D mesh, it can be expressed in the most basic

[1] More details on XFEM is given in Section 2.2

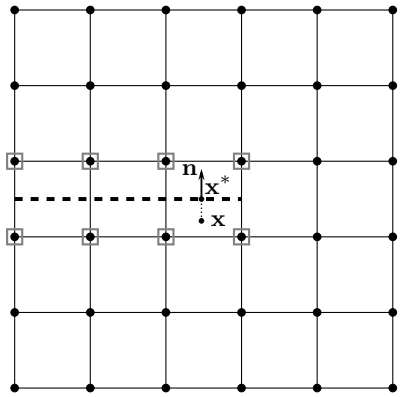

Figure 2.1: *FE mesh with an embedded crack shown with a dashed line. The enriched nodes marked with squares. For an arbitrary point* $\mathbf{x}$ *in the domain, the corresponding* $\mathbf{x}^*$ *and* $\mathbf{n}$ *at* $\mathbf{x}^*$ *are shown that is used in the Heaviside function calculation.*

case as

$$\mathbf{u}^{\mathrm{FE}}(\mathbf{x}) = \underbrace{\mathbf{N}(\mathbf{x})\mathbf{a}}_{\text{standard}} + \underbrace{\mathbf{N}(\mathbf{x})H(\mathbf{x})\mathbf{b}}_{\text{enrichment}}, \tag{2.1}$$

where $\mathbf{N}$ contains shape functions, $\mathbf{a}$ consists of nodal displacements, and $\mathbf{x}$ shows spatial coordinates. Also, $\mathbf{b}$ contains enrichment nodal values, and $H(\mathbf{x})$ is the Heaviside function defined as

$$H(\mathbf{x}) = \begin{cases} 1 & \text{for } (\mathbf{x}-\mathbf{x}^*)\cdot\mathbf{n} > 0 \\ 0 & \text{for } (\mathbf{x}-\mathbf{x}^*)\cdot\mathbf{n} < 0 \end{cases}. \tag{2.2}$$

Here, $\mathbf{x}^*$ is the point on the crack closest to $\mathbf{x}$, and $\mathbf{n}$ denotes the unit outward normal to the crack at $\mathbf{x}^*$.

XFEM still requires mesh refinement in the crack area, but the mesh does not need to conform to the crack geometry. However, if a crack crosses an element very close to one of its nodes or coincides with element edges, it can cause numerical issues. As a result, the method allows for modelling the crack (almost) independently of the FE mesh and makes crack geometry modifications much easier compared to previous methods. For this, XFEM has become a very popular method in crack propagation analyses. It has been applied in different areas, and more enrichment terms have been proposed to capture more specific phenomena related to the problem at hand and to improve the numerical convergence of the method. For instance, it is possible to explicitly incorporate the singular fields. This also allows the crack tip/front to reside within an element. More details are given in e.g., [31].

As RCF cracks experience large shear and compressive loads, another important aspect of RCF crack modelling in FE analyses is the crack face constraints. Contact constraints at the crack faces in the normal direction ($\hat{\mathbf{e}}_\perp$ in Fig. 2.2) are employed to avoid crack

face penetrations. Crack face friction is considered by modelling the relation between tangential traction and slip, i.e., relative displacements of contacting faces. A more detailed description of contact constraints is given in [32].

2.3 Prediction of mixed-mode crack growth

There are three modes of crack growth: opening mode (mode I, tensile growth), sliding mode (mode II, shear growth), and tearing mode (mode III, shear growth) [33]. A crack can grow in one of these modes or in a combination of modes. Abundant studies in the literature focus on tensile growth since the majority of practical cases occur in this mode. However, this is not the case for RCF cracks. The loading of such cracks is in general in mixed-mode.

In Paris law [34], the fatigue crack growth rate is evaluated from the range of the SIF through a power law and mode I growth is typically presumed. This is one of the most commonly used crack growth laws even today. Conceptually, the criteria developed in the literature for fatigue crack growth under mixed-mode loading can generally be divided into three categories: stress-, energy- and displacement-based. Note that, the majority of the criteria in the literature are developed within the scope of LEFM, and generally presume proportional and planar loading.

Stress-based criteria propose that a crack grows in the direction defined based on a stress-based parameter. Two of the most commonly used criteria are Maximum Tangential Stress (MTS) and Maximum Shear Stress (MSS) [35]. In short, the MTS criterion assumes crack growth perpendicular to the maximum tangential stress[2] and MSS postulates that crack grows in the direction of the maximum shear stress. Both of the criteria were originally developed for static/monotonic analysis, but common practice is to employ the range of stress parameters, often described in terms of SIFs, to adapt these criteria for fatigue crack growth analysis, e.g., the MTS range criterion proposed in [36]. Different extensions of each of these criteria exist in the literature to account for different phenomena. For instance, crack closure can be considered by applying effective SIFs, see e.g., [37]. In addition, there are some other criteria in the literature that use similar concepts as the MTS and MSS criteria. For example, a criterion in [38] suggested that a crack in 3D propagates perpendicular to the direction of the maximum principal stress. Regarding the performance of these criteria, MTS-based criteria have good accuracy for the predictions in mode I dominated crack growth [39], whereas their performance worsens as the crack shear loading increases [40, 41]. On the other hand, MSS-based criteria can predict shear-driven growth accurately [42] but are inaccurate for tensile growth [43]. In short, these criteria typically give more reliable results when one mode dominates crack propagation. For crack growth rate evaluations under mixed-mode loading, these criteria typically employ a Paris-type equation with an equivalent SIF, see e.g., [44, 45, 46]. In this regard, Qian

[2]Tangential stress is also known as hoop stress and circumferential stress.

and Fatemi [47] and Richard et al. [48] reviewed some of the most common criteria in the literature and briefly discussed their underlying assumptions.

Energy-based criteria are set out from the energy release rate [49], which is a scalar quantity defined as the rate of change in potential energy with respect to a crack extension. Also, the term crack driving force is commonly used in the literature as a vectorial counterpart of the energy release rate. The J-integral [21, 22] is a measure that is usually used in this type of criteria. Although this measure was originally proposed for a non-linear elastic case in [22], it can, to some extent, also be applicable to elastic-plastic conditions. A cyclic J-integral (ΔJ) that considers elastic-plastic responses can be employed for fatigue crack growth, see e.g., [50, 51]. This criterion can (to some extent) deal with multiaxial loading but it does not provide any information on growth direction in itself. However, it can be used with e.g., virtual crack extension techniques [52, 53] to find the direction that maximizes the energy release rate for propagating the crack. Another criterion in this category is the Minimum Strain Energy Density (MSED) criterion [54, 55], which assumes crack growth in the direction that minimizes the strain energy density function, S. MSED-based criteria are able to predict mode I dominated crack growth with good accuracy [39], but they cannot accurately predict under mode II dominant conditions [40, 41]. Regarding the crack growth rate, a Paris-type equation is usually employed and the SIF range in the equation is replaced by an energy-based parameter, e.g., ΔJ or ΔS.

During the recent decades, the concept of the Configurational Forces (CF) (or material forces) [56], which can be considered as a vectorial extension of the energy release rate, was employed to evaluate crack driving forces [57]. In this approach, the crack driving force can give information about both the rate and direction of crack growth. In addition, CF criteria can account for various phenomena such as crack closure, crack face friction and inelastic material behaviour. Thus, it attracted great attention from researchers in the field. However, it has been shown that the CF criteria are typically not very numerically stable. For instance, an RCF crack propagation using a CF criterion in [58] showed that the perpendicular component of the employed CF criterion is heavily mesh-dependent. The pathological mesh sensitivity was solved in [59] by adding regularization in terms of gradient-enhanced plasticity into the criterion. A CF criterion was used in [43] to simulate four mixed-mode fatigue crack growth experiments in 2D (tensile growth under mode I-dominated crack loading, tensile growth under mixed-mode crack loading, stable shear growth under non-proportional loading, and shear growth followed by crack kinking to tensile growth). It demonstrated that the performance of the criterion decreases as shear loading increases. It is also sensitive to the material model used in the simulations, and the approach for the evaluation of crack driving force (i.e., viscous or rate-independent).

Displacement-based criteria are usually developed based on the crack face displacements near the crack tip, i.e., Crack Tip Opening Displacement (CTOD or δ_{I}) and Crack Tip Sliding Displacement (CTSD or δ_{II}). They stem from [60], but there are very few displacement-based criteria in the literature for mixed-mode loading due to difficulties in measuring δ_{I} and δ_{II} [61]. Although δ_{I} and δ_{II} are related to SIFs in LEFM, the criteria are

also applicable to, e.g., elastic-plastic responses, since the criteria depend only on δ_{I} and δ_{II}. However, the criteria are sensitive to how δ_{I} and δ_{II} are evaluated. The Vector Crack Tip Displacement (VCTD) criterion [62] was proposed under proportional loading, based on the assumption that cyclic deformations are the microscopic mechanism for fatigue crack growth. Hence, it was concluded that the crack tip displacements represent the condition at the crack tip and can be used to define the propagation. The fatigue crack growth direction in the VCTD criterion is determined using the range of crack face displacements, i.e., $\Delta\delta_{\mathrm{I}}$ and $\Delta\delta_{\mathrm{II}}$. This is defined in the crack local coordinate system at the crack tip (as shown in Fig. 2.2) as $\vartheta = \arcsin(\Delta\delta_{\mathrm{II}}/\Delta\delta)$, where $\Delta\delta = \sqrt{\Delta\delta_{\mathrm{I}}^2 + 2\Delta\delta_{\mathrm{I}}\Delta\delta_{\mathrm{II}} + 2\Delta\delta_{\mathrm{II}}^2}$. The analytical crack growth direction and rate predictions of the VCTD criterion show good agreement with experimental results under proportional mixed-mode loading [62]. In simulating four fatigue tests in [43], a modification of the VCTD criterion yielded promising crack growth direction results for a linear elastic material model and it was also shown that modelling the cyclic elastic-plastic material response did not improve the accuracy of the predictions. It should be noted that using the crack driving displacement from the VCTD criterion in a Paris-type equation for rate predictions in some cases can overestimate the predicted growth rates, see e.g., [63].

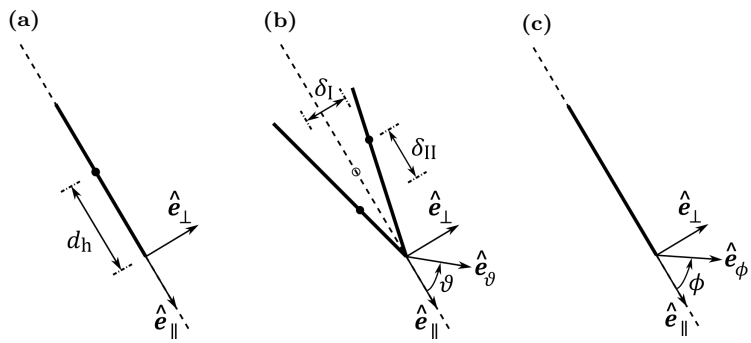

Figure 2.2: *Illustration of crack growth variables. Crack local coordinate system* $(\hat{\mathbf{e}}_{\parallel}, \hat{\mathbf{e}}_{\perp})$ *at the crack tip for an inclined crack is shown. The dashed line indicates the orientation of the undeformed crack. (a) Undeformed closed crack. (b) Crack tip displacements and instantaneous crack growth direction,* ϑ*, for a loaded crack. (c) Crack growth direction for the entire load cycle,* ϕ*. Adapted from* ***Paper A****.*

Another criterion, the maximum crack growth rate criterion [64, 65], assumes that the crack grows in the direction that maximizes the crack growth rate. The criterion performs well in shear-dominated crack growth and can handle non-proportional loading. However, the performance of the criterion worsens for a higher degree of mixed-mode I and II loading [64].

Based on the above discussion and the challenges mentioned in [66], there are still issues regarding the analysis of fatigue crack growth under mixed-mode loading which are not fully addressed in the literature. The situation for RCF cracks is even more complex

[9] since the (frictional) rolling contact conditions impose a non-proportional multiaxial stress/strain state, which exerts compression and mixed-mode deformations on these cracks. The formation of large plastic deformation is also present near the contact surfaces. In non-proportional mixed-mode loading, challenges such as high mode mixity, cyclic plasticity, crack closure, and variable mode mixity along the crack front need further investigation, and there is no (globally) accepted crack driving force parameter in the literature, see [67]. In addition, one way to account for the variation of phase angle between the modes in the case of non-proportional loading is to consider an accumulation of instantaneous contributions. However, there are challenges in formulating the accumulation scheme, and in the scheme calibration that requires (substantial) experimental data.

In railways, shorter RCF cracks grow mainly under shear while the larger ones can deviate to tensile growth due to the longitudinal tensile thermal and bending loads that exist in the rails [68]. Therefore, it is crucial for the crack growth direction criterion to also be able to capture the transition from shear to tensile growth.

Stress-based criteria are not suitable for these cracks due to their poor predictive performance under a high degree of mixed-mode loading. Moreover, most of these criteria can only be employed in LEFM analyses because of the employment of elastic response with small-scale yielding assumption. Although energy-based criteria can theoretically be a fascinating option for RCF cracks, more development is needed to address some practical issues regarding the reliability and robustness of the numerical results. Displacement-based criteria do not have any limiting theoretical assumption in order to be applicable to RCF cracks and they have shown promising results under stable shear growth, for the transition from shear to tensile growth, and during tensile growth for both proportional and non-proportional loadings [43, 69].

2.4 Wheel–rail contact modelling

The wheel–rail contact generates a stress field that drives the growth of surface initiated cracks, particularly for smaller cracks. In the contact interface, contact pressure, and longitudinal and lateral tractions can generally be present. Although normal and tangential tractions are in general coupled, the influence of the tangential traction on the normal contact pressure distribution and the contact patch size is small for elastic bodies in contact (zero for elastically compliant contacting bodies[3]) [70]. As a result, a common approach is to first solve the normal contact problem to evaluate the magnitude and distribution of the contact pressure. The tangential problem is then solved using the results of the normal contact and the relative velocity between the contacting bodies known as creepage. There is a lot of research in the literature to investigate different aspects of contact problems, see e.g., Johnson [70] and Kalker [71] books on this topic.

[3]This requires that the contacting bodies have the same elastic constants defined in terms of shear modulus G and Poisson's ratio ν, i.e., $\frac{G_1}{1-2\nu_1} = \frac{G_2}{1-2\nu_2}$.

Analytical solutions to the rolling contact problem can provide generally good insights into the subject in a computationally efficient way. Hertzian theory [5] is one of the most commonly used among these solutions. The theory considers an elliptical contact patch with semi-axes a and b with a semi-ellipsoid pressure distribution, see Fig. 2.3, for normal wheel–rail contact under the following assumptions [70]:

- Homogeneous isotropic linear elasticity.
- Linear kinematics, i.e., small deformation theory is valid.
- Constant curvature, i.e., contacting surfaces can be described by quadratic functions within the contact patch.
- Half-space condition, i.e., contact patch size is small compared to the dimensions of the contacting bodies.
- Perfectly smooth (frictionless) contact surfaces.

The contact patch semi-axes, a and b, are evaluated following [72], and depend on the loading, and geometrical and elastic properties of the contacting bodies.

For 2D investigations, an approach proposed in [70] for two cylindrical bodies with parallel axes in contact can be used. This condition gives a contact width, b, with an elliptical pressure distribution that extends over a strip in the thickness direction (rectangular contact patch).

The Hertzian theory assumptions are usually violated (to some extent) in the wheel–rail contact scenarios. To highlight some of the violated situations in railways, plastic deformations can occur for heavy wheel loads. The wheel and rail profiles have different curvatures in different parts of their profile, especially at the gauge shoulder [73]. Conformal contact (large contact area) can also occur in the case of flange contact. Moreover, two-point contact can occur e.g., in curve negotiations. However, the theory can still be beneficial as an approximation, especially in computationally demanding simulations, where computational efficiency is an important parameter. Moreover, the theory laid a foundation for more advanced (normal) contact theories.

The modified version of Kalker's exact contact theory, also known as Li-Kalker theory, [74] can deal with non-elliptical contact patches, multiple contact points, and conformal contact. However, this theory needs (relatively) intensive computations. STRIPES [75] is a computationally efficient semi-Hertzian approach, which divides the contact patch into strips in the rolling direction of the wheel and applies a Hertzian-based pressure in the direction of rolling on each strip locally. Investigations in [76] show that the method is more accurate and still fast for cases that Hertzian theory cannot handle.

There are also several methods for solving the tangential rolling contact problem. Carter's method [70] and Kalker's simplified and exact theories [77, 71] are three of the most commonly used approaches in the literature. Note that the tangential stress, p_{t}, reaches full slip conditions, i.e., $p_{\mathrm{t}} = f_{\mathrm{wr}} p_{\mathrm{n}}$, when the creepage is sufficiently high. Here,

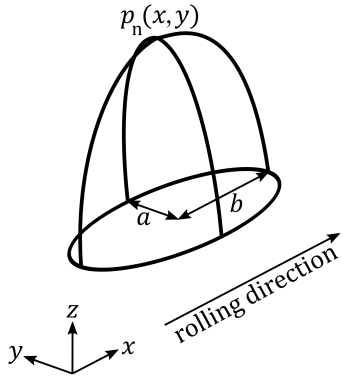

Figure 2.3: *Illustration of a Hertzian pressure distribution, $p_n(x,y)$, with semi-axes a and b.*

f_{wr} is the wheel–rail traction coefficient and p_n shows normal pressure between contacting bodies. More details regarding available wheel–rail contact models are given in [78].

3 Numerical framework

3.1 FE model

For 2D investigations in **Papers A** and **B**, a rectangular (rail) part with the width of $w = 300\,\text{mm}$ and the height of $h = 100\,\text{mm}$ is used as the FE domain, see Fig. 3.1. Plane strain conditions are presumed and the bottom edge of the model is clamped in the global y-direction. Three-noded (linear) triangular elements are used in **Paper A** and 8-noded (second-order) quadrilateral elements are employed in **Paper B** to discretise the FE domain.

A 300 mm long and 172 mm high 60E1 rail profile [79] is used as the FE domain for 3D studies in **Papers C** and **D**, see Fig. 3.2. 8-noded (linear) hexahedral elements, also known as brick elements, are used for discretisation. The bottom surface of the model is clamped in the global x- and y-directions. In this thesis, a linearly elastic material model is used. More details regarding the FE models are given in **Papers A**–**D**.

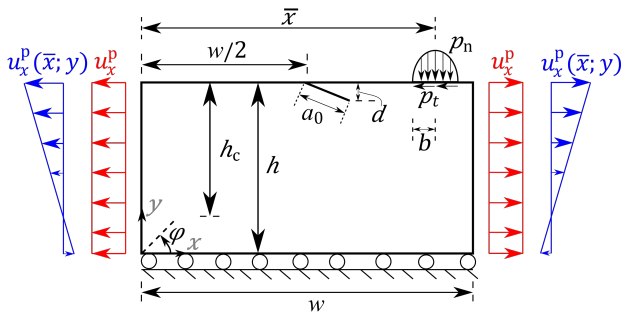

Figure 3.1: *A sketch of a 2D rail part with an isolated surface-breaking inclined crack subjected to a Hertzian contact load (p_n,p_t) and constant longitudinal prescribed displacements u_x^p (red), or boundary displacements $u_x^p(\bar{x};y)$ corresponding to bending (blue). Adapted from **Paper B**.*

3.2 Crack modelling

A discrete crack modelling approach with remeshing is adopted in the 2D investigations in **Papers A** and **B**. As shown in Fig. 3.1, an initial crack with an inclination of $\varphi_0 = -25°$ and an initial crack length of $a_0 = 4.3\,\text{mm}$ with the tip initially at a depth of $d = 2\,\text{mm}$ is considered. The crack is propagated in an unbiased fashion (i.e., not following a prescribed path) in the direction predicted by an accumulative VCTD criterion, see Section 3.4, in the 2D studies (**Papers A** and **B**). The accumulated growth for multiple cycles is

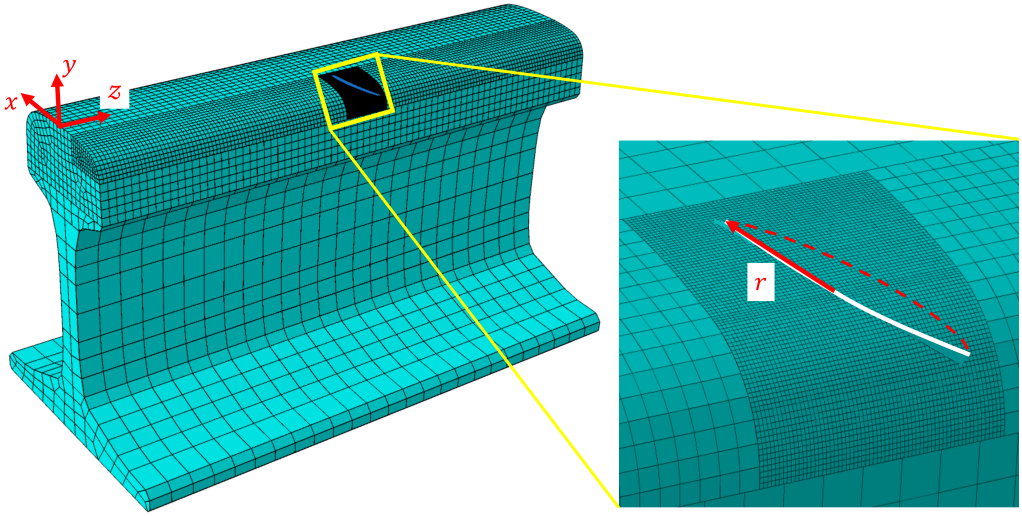

Figure 3.2: *The FE mesh used for the 60E1 rail profile features a semi-circular, surface-breaking inclined gauge corner crack with a radius of r. A detailed view of the mesh in the cracked area, highlighted by a box on the global mesh, is provided. From* ***Paper D****.*

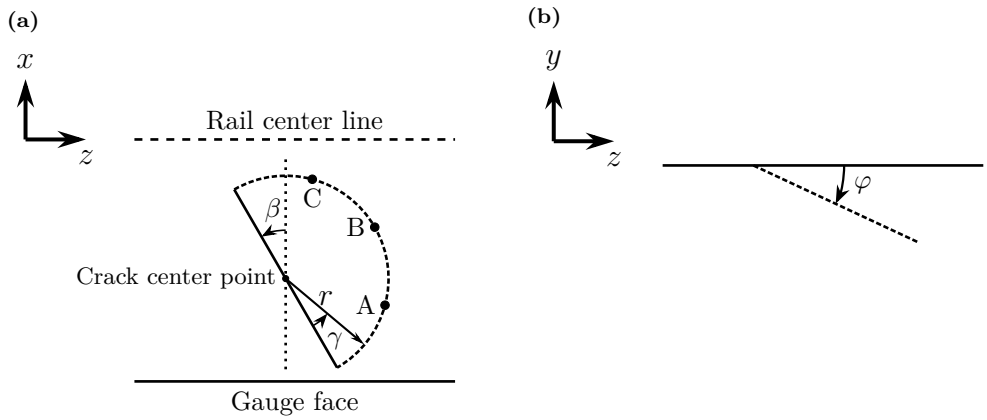

Figure 3.3: *Crack plane inclination (defined by angles φ and β) w.r.t. the rail. (a) Top view (xz-plane). Point A is located at the gauge side ($\gamma = 45°$), B at the middle of the crack front ($\gamma = 90°$), and C at the center side ($\gamma = 135°$). (b) Side view of the cracked rail head (yz-plane). Adapted from* ***Paper D****.*

simulated by repeating the process for each load cycle. In these studies, the crack growth direction and rate are predicted in an 'uncoupled' way, i.e., the length of the incremental propagation of the crack is a pure discretisation parameter (rather than representing a certain number of load cycles).

XFEM is used in the 3D investigations in **Papers C** and **D**. Fig. 3.2 shows the

individual surface-breaking inclined crack considered at the rail gauge corner in the middle of the rail section. The crack is quasi semi-circular with a radius r. The crack plane is assumed to have an inclination of φ w.r.t. the z-axis and β w.r.t. the x-axis, see Fig. 3.3. The crack is considered stationary in the 3D studies (**Papers C** and **D**). Results are evaluated at three different points along the crack front: point A on the gauge side with $\gamma = 45°$, point B at the middle of the crack front with $\gamma = 90°$, and point C on the center side with $\gamma = 135°$, as shown in Fig. 3.3a. Four crack radii ($r = 3,\ 5,\ 9,\ 13$ mm) are considered.

In this thesis, similar to the FE mesh shown in Fig. 3.2, a mesh refinement close to the crack area, with no special or singular elements around the crack tip, is employed. To apply contact constraints at the crack faces in the normal direction, a penalty formulation is employed in **Papers A**–**D**. For the tangential direction, frictionless crack faces are considered in **Papers A**, **C**, and **D**, while crack face friction using a Coulomb friction model is employed in **Paper B**. In this model, the tangential traction between two contacting surfaces, p_t, is evaluated as

$$\begin{cases} |p_\mathrm{t}| \leq \mu_\mathrm{CF}\, p_\mathrm{n} & v_\mathrm{t} = 0 \quad \text{(stick condition)} \\ p_\mathrm{t} = -\mu_\mathrm{CF}\, p_\mathrm{n} \frac{v_\mathrm{t}}{|v_\mathrm{t}|} & v_\mathrm{t} \neq 0 \quad \text{(slip condition)} \end{cases}. \tag{3.1}$$

Here, μ_CF and p_n are the friction coefficient and normal contact pressure between the surfaces, respectively, and v_t denotes relative sliding velocity.

3.3 Operational loads

In this thesis, three loads are considered: contact loading due to a wheel passage, longitudinal bending, and thermal loading. The influence of each load on predicted crack growth direction and rate is evaluated independently and in combinations. A brief description is given below. Details are found in **Papers A**–**D**.

3.3.1 Contact load

Hertzian theory is employed for solving the normal rolling contact problem in this thesis due to its computational efficiency. For the 2D investigations in **Papers A** and **B**, a 2D Hertzian approach as proposed in [70] for cylindrical bodies with parallel axes in contact is used. The contact patch width, b, is evaluated following [72]. In the 3D investigations in **Papers C** and **D**, a semi-ellipsoid load distribution is applied over an elliptical contact patch with semi-axes a and b, as computed following [72].

For all the studied cases in **Papers A**–**D**, wheel–rail longitudinal stresses are evaluated presuming full slip conditions, and the lateral tractive stresses are not considered. The influence of varying contact loads is investigated in **Papers A**, **B**, and **D**.

3.3.2 Rail bending load

A passing wheelset induces bending in the rails. In this thesis, longitudinal bending is considered, and evaluated using the in-house code DIFF [80]. The evolution of bending moment as a wheel load traverses a track section, obtained from DIFF simulations, is applied as boundary displacements on the vertical side edges of the model, see Fig. 3.1 for the 2D model. For this, the rail model is considered as an Euler–Bernoulli beam, and boundary displacements are evaluated using the moment–curvature relation. Further, it is assumed that the crack is located at the midspan of a sleeper bay for 2D investigations in **Papers A** and **B**, and above a sleeper for 3D investigations in **Papers C** and **D** as this location is more critical for crack growth in a rail head. In addition, the influence of track support conditions and varying wheel loads is investigated in **Paper D**.

3.3.3 Thermal load

A continuously welded rail experiences longitudinal thermal loads due to the variation of the ambient temperature from the stress-free temperature. This load is applied as prescribed uniform displacements acting on the vertical side edges of the rail part using a linear thermoelasticity assumption, as shown in Fig. 3.1 for the 2D model. Tensile thermal load, i.e., temperature drop due to cold climate, is considered in **Papers A**–**D**, and compressive thermal load is investigated in **Paper B** to show the performance of the framework under this load. The influence of varying thermal loads is investigated in **Paper D**.

3.4 Prediction of crack growth direction

In this thesis, the VCTD criterion has been chosen to predict crack growth directions. The employed criterion is a modification of the original VCTD criterion [62] that considers an accumulation scheme to account for non-proportional loading [43].

The accumulated VCTD criterion proposed in [43] is used in **Paper A**. For this, crack face opening displacement, $\delta_{\mathrm{I}}(t)$, and crack face sliding displacement, $\delta_{\mathrm{II}}(t)$, are computed at a distance d_{h} from the crack tip for each time instance t of the load cycle. This can be expressed as the difference between the top and bottom surface crack face displacements ($\vartheta = \pi$, and $\vartheta = -\pi$, respectively as shown in Fig. 2.2), i.e.,

$$\delta_{\mathrm{I}}(d_{\mathrm{h}},t) = u_{\perp}(d_{\mathrm{h}},\pi,t) - u_{\perp}(d_{\mathrm{h}},-\pi,t), \qquad \delta_{\mathrm{II}}(d_{\mathrm{h}},t) = u_{\parallel}(d_{\mathrm{h}},\pi,t) - u_{\parallel}(d_{\mathrm{h}},-\pi,t). \quad (3.2)$$

The 'amplitudes' of $\delta_{\mathrm{I}}(t)$ and $\delta_{\mathrm{II}}(t)$ are defined using mid-values over the load cycle, $\overline{\delta}_{\mathrm{I/II}} = \frac{1}{2}\left[\max_t\left(\delta_{\mathrm{I/II}}(t)\right) + \min_t\left(\delta_{\mathrm{I/II}}(t)\right)\right]$, as $\tilde{\delta}_{\mathrm{I/II}}(t) = \delta_{\mathrm{I/II}}(t) - \overline{\delta}_{\mathrm{I/II}}$.

The instantaneous crack growth direction, $\vartheta(t)$, in the crack local coordinate system shown in Fig. 2.2, and the instantaneous crack driving displacement, $\tilde{\delta}(t)$, are evaluated

as

$$\vartheta(t) = \arcsin\left(\frac{-\tilde{\delta}_{\mathrm{II}}(t)}{\tilde{\delta}(t)}\right), \tag{3.3}$$

and

$$\tilde{\delta}(t) = \sqrt{\langle\tilde{\delta}_{\mathrm{I}}(t)\rangle^2 + 2\langle\tilde{\delta}_{\mathrm{I}}(t)\rangle|\tilde{\delta}_{\mathrm{II}}(t)| + 2\tilde{\delta}_{\mathrm{II}}(t)^2}, \tag{3.4}$$

where $\langle\bullet\rangle = \frac{1}{2}\left[\bullet + |\bullet|\right]$ are Macaulay brackets.

The crack driving displacement, $\boldsymbol{\Delta}\mathbf{a}$, is evaluated from the accumulation of instantaneous contributions assuming a rate-independent response for the entire load cycle. More specifically, the crack driving displacement is evaluated as the maximum of two trial crack driving displacements corresponding to presumed positive and negative growth directions, $\boldsymbol{\Delta}\mathbf{a}^+$ and $\boldsymbol{\Delta}\mathbf{a}^-$ respectively,

$$\boldsymbol{\Delta}\mathbf{a} = \underset{\boldsymbol{\Delta}\tilde{\mathbf{a}}\in\{\boldsymbol{\Delta}\mathbf{a}^+,\boldsymbol{\Delta}\mathbf{a}^-\}}{\operatorname{argmax}} \|\boldsymbol{\Delta}\tilde{\mathbf{a}}\|, \quad \boldsymbol{\Delta}\mathbf{a}^{+/-} = \int_0^{T_c} \langle\frac{\mathrm{d}\tilde{\delta}(t)}{\mathrm{d}t}\rangle \hat{\mathbf{e}}_\vartheta(t) f^{+/-}(t)\,\mathrm{d}t. \tag{3.5}$$

Here, $\hat{\mathbf{e}}_\vartheta(t)$ is the unit vector in the direction of the instantaneous crack growth direction $\vartheta(t)$, see Fig. 2.2b. Further, $f^+(t)$ and $f^-(t)$ apply the 'reversed shear' condition and are defined as

$$f^+(t) = \begin{cases} 0 & \tilde{\delta}_{\mathrm{II}} < 0 \text{ and } \frac{\delta_{\mathrm{I}}}{|\delta_{\mathrm{II}}|} \leq \psi \\ 1 & \tilde{\delta}_{\mathrm{II}} \geq 0 \text{ or } \frac{\delta_{\mathrm{I}}}{|\delta_{\mathrm{II}}|} > \psi \end{cases}, \quad f^-(t) = \begin{cases} 0 & \tilde{\delta}_{\mathrm{II}} > 0 \text{ and } \frac{\delta_{\mathrm{I}}}{|\delta_{\mathrm{II}}|} \leq \psi \\ 1 & \tilde{\delta}_{\mathrm{II}} \leq 0 \text{ or } \frac{\delta_{\mathrm{I}}}{|\delta_{\mathrm{II}}|} > \psi \end{cases}, \tag{3.6}$$

where ψ is the reversed shear threshold parameter. This parameter is used to account for crack face locking by restricting the contribution of 'reversed shear' instances. Here, crack face locking is defined as in [81], meaning that a part of the crack is active (has slip between crack faces) at each time instant and there are no relative displacements between the closed crack faces for inactive part(s) of the crack. Also, 'reversed shear' refers to a shear deformation with the opposite sign to the presumed growth direction.

The accumulated crack propagation direction for the entire load cycle ϕ in the crack local coordinate system, shown in Fig. 2.2c, is computed as a unit vector in the direction of the crack driving displacement vector, i.e.,

$$\hat{\mathbf{e}}_\phi = \frac{\boldsymbol{\Delta}\mathbf{a}}{\|\boldsymbol{\Delta}\mathbf{a}\|}. \tag{3.7}$$

A modification in the criterion has been proposed in **Paper B**. This modified version is then used in **Papers B–D**. In short, the modification neglects the 'reversed shear' condition and thereby, Eqs. (3.5) and (3.6) are replaced by

$$\boldsymbol{\Delta}\mathbf{a} = \int_0^{T_c} \langle\frac{\mathrm{d}\tilde{\delta}(t)}{\mathrm{d}t}\rangle \hat{\mathbf{e}}_\vartheta(t)\,\mathrm{d}t. \tag{3.8}$$

Crack face displacements, $\delta_{\mathrm{I}}(t)$ and $\delta_{\mathrm{II}}(t)$, in Eq. (3.2) are computed directly from FE resolved displacement fields in **Papers A** and **B** (2D investigations) and from SIFs, which are evaluated following [24], in **Papers C** and **D** (3D investigations). For more information regarding the detailed formulae of the employed criteria, see **Papers A**–**D** [1].

Remark. Eqs. (3.5) and (3.8) result in a rate-independent formulation related to the range of $\tilde{\delta}$. As an illustration, in the scalar case (considering constant direction),

$$\int_0^{T_c} \langle \frac{\mathrm{d}\tilde{\delta}(t)}{\mathrm{d}t} \rangle \, \mathrm{d}t = \max_{0<t<T_c} \big(\tilde{\delta}(t)\big) - \min_{0<t<T_c} \big(\tilde{\delta}(t)\big) = \Delta\tilde{\delta}. \tag{3.9}$$

Hence, the loading is proportional to the range $\Delta\tilde{\delta}$ and independent of the load cycle duration, T_c.

3.5 Prediction of crack growth rate

Paris-type laws are used to predict crack growth rates. Two versions are employed to account for various mode interactions. The zero mode interaction is assumed (lower estimate 'lo') using

$$\left(\frac{da}{dN}\right)_{\mathrm{lo}} = C(\Delta K_{\mathrm{I}})^m + C(\Delta K_{\mathrm{II}})^m + C\left(\frac{\Delta K_{\mathrm{III}}}{\sqrt{1-\nu}}\right)^m, \tag{3.10}$$

and full mode interaction (upper estimate 'up') is considered using

$$\left(\frac{da}{dN}\right)_{\mathrm{up}} = C(\Delta K_{\mathrm{eq}})^m, \quad \text{with} \quad \Delta K_{\mathrm{eq}} = \sqrt{\Delta K_{\mathrm{I}}^2 + \Delta K_{\mathrm{II}}^2 + \frac{1}{1-\nu}\Delta K_{\mathrm{III}}^2}. \tag{3.11}$$

Eqs. (3.10) and (3.11) are used in **Papers C** and **D** (3D investigations). $\Delta K_{\mathrm{III}} = 0$ is presumed to obtain the equations in **Paper B** (2D investigations) with the history of SIFs evaluated from a direct displacement-based approach. For more information on growth rate predictions, see **Papers B**–**D**.

Remark. The chosen expression incorporating ΔK_{III} in the lower estimate of crack growth rate (Eq. (3.10)) leads to the explicit inequality $\left(\frac{da}{dN}\right)_{\mathrm{up}} \geq \left(\frac{da}{dN}\right)_{\mathrm{lo}}$, given that SIF ranges for all three modes are non-negative ($\Delta K = \max_t(K(t)) - \min_t(K(t))$).

[1] Note that there is a sign error in the formula presented for crack face displacements in **Paper A**.

4 Summary of appended papers

4.1 Preliminaries

In **Papers A–D**, the FE model briefly described in Chapter 3 was implemented in the commercial FE software ABAQUS/CAE [82], and post-processing was conducted in MATLAB [83]. The overall contents of the appended papers are indicated in Table 4.1. Highlighted results of each paper are briefly described in the following.

Table 4.1: Overall contents of the appended papers.

	model dimension	crack modelling	growth direction	growth rate	varying loads	crack face friction
Paper A	2D	propagating	✓		✓	
Paper B	2D	propagating	✓	✓	✓	✓
Paper C	3D	stationary	✓	✓		
Paper D	3D	stationary	✓	✓	✓	

4.2 Paper A: Numerical predictions of crack growth direction in a railhead under contact, bending and thermal loads

The main objective of this paper is to establish a numerical framework for predicting the crack growth path in a 2D rail model under operational loads simplified to 2D. For this, a numerical framework for a 2D linear elastic model of a rail under plane strain conditions with an isolated surface-breaking frictionless crack has been developed. The influence of wheel–rail contact load, rail bending and tensile thermal loads (individually and in combinations) on predicted crack paths is investigated. The inclined crack is propagated into the rail in an unbiased manner (i.e., not following a prescribed path) based on the predicted growth direction at the end of each load cycle using an accumulative VCTD criterion as proposed in [43] (see Section 3.4). In addition, the effect of the employed value of the reversed shear threshold parameter, ψ, on the predicted crack paths is investigated.

To model the crack growth under winter conditions in rails, a tensile thermal load in combination with a moving Hertzian contact load of varying magnitude and a wheel–rail traction coefficient of $f_{\mathrm{wr}} = 0.3$ was studied. As shown in Fig. 4.1, the crack tends to grow towards a shallower path as the contact load magnitude increases. This change in the crack path happens gradually. Results have the same trend for both ψ values studied. It is thus concluded that the employed value for the reversed shear threshold parameter, ψ, does not have a strong influence on the predicted crack paths for these load combinations.

To mimic rail bending by passing wheels, a combined load of bending and a moving contact load of varying magnitude with a traction coefficient of $f_{\mathrm{wr}} = 0.3$ was investigated.

It is observed in Fig. 4.2 that the combinations of bending and low contact loads result in crack path predictions similar to those of pure bending, while the predicted crack paths for higher contact loads in combination with bending are closer to the crack path for a pure contact load. The change in the crack path happens abruptly. The trends are similar between $\psi = 0.001$ and $\psi = 0.01$. However, the jump between the paths occurs at a lower contact load for $\psi = 0.001$. This shows that the predicted crack paths for combined bending and contact loads are somewhat sensitive to the employed ψ value.

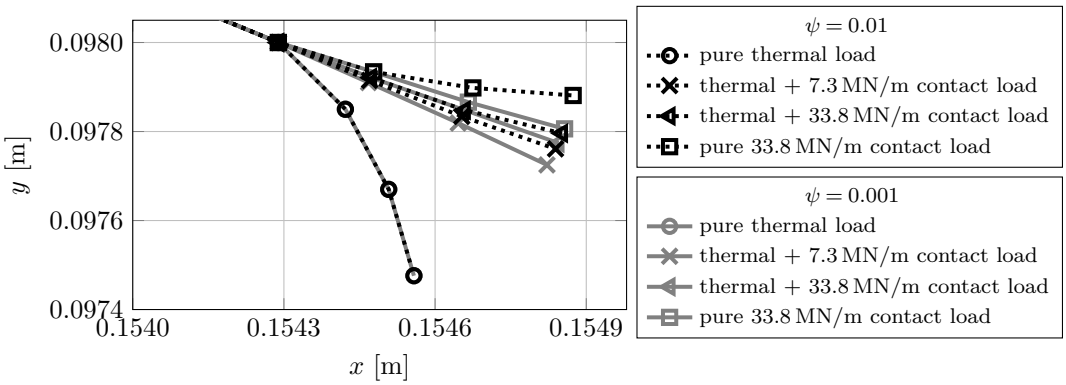

Figure 4.1: *Predicted crack paths for a frictionless crack under tensile thermal ($\Delta T = -20\,^{\circ}\mathrm{C}$) load in combination with different contact load magnitudes with $f_{\mathrm{wr}} = 0.3$. Corrected from* ***Paper A****.*

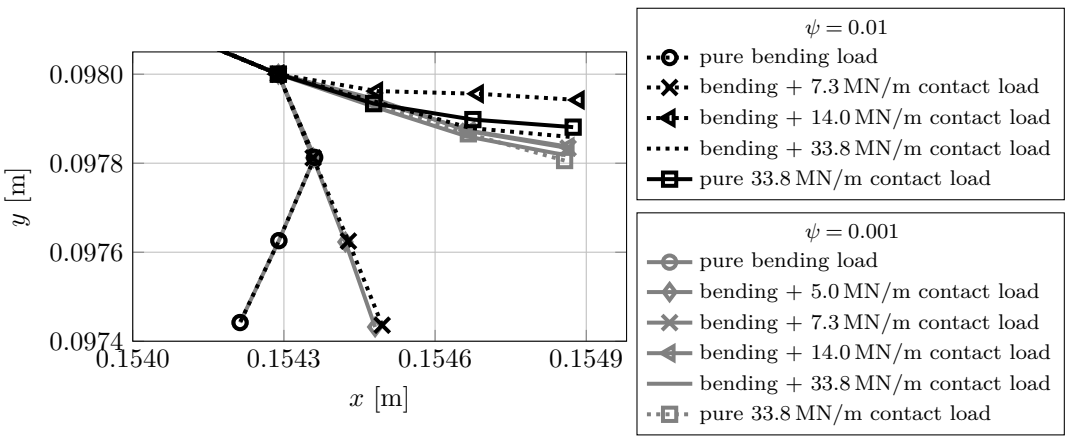

Figure 4.2: *Predicted crack paths for a frictionless crack under combined bending and varying contact load magnitudes with $f_{\mathrm{wr}} = 0.3$. Adapted from* ***Paper A****.*

4.3 Paper B: Numerical prediction of railhead rolling contact fatigue crack growth

The main goal of the paper is to further develop the proposed numerical framework in **Paper A** to account for crack face friction and also to predict crack growth rates. The crack face friction has been modelled using the Coulomb model, and the crack growth rate has been evaluated employing two Paris-type equations described in Section 3.5. In this study, two modifications are proposed for the numerical framework. Firstly, removing the reversed shear condition in the accumulated VCTD criterion leads to a better match with results from a twin-disc experiment and more physically sound predictions under combined loads. Also, a change in the mid-value computations over a load cycle is considered only under combined thermal and contact load, which is due to the difference in the time scale of the contact and thermal loads (see discussion in **Paper B**). In addition, the influence of a compressive thermal load is studied.

Similar load combinations as used in **Paper A** are employed to investigate the influence of the crack face friction on the crack growth. The predicted crack paths for frictional and frictionless cracks under combined thermal and contact loads are shown in Fig. 4.3a. A similar trend is seen for the results in both cases with a little more tendency towards transverse growth for the thermal and 7.3 MN/m contact load in the frictionless crack. It is thus concluded that the crack face friction has a moderate influence on the predicted crack path. Further, the friction reduces the crack growth rate as shown in Fig. 4.3b.

A similar study was conducted for combined bending and contact loads. Predicted crack paths are presented in Fig. 4.4a. The crack grows deeper into the rail in the presence of crack face friction for this load combination. In addition, the abrupt change between the predicted frictionless paths under this load combination seen in Fig. 4.2 is replaced by a more gradual change. Fig. 4.4b shows that friction reduces the crack growth rate.

Note that there is always a need for a (more or less arbitrary) scale factor between a 2D model and a 3D wheel–rail contact load. This factor can have a large influence on the predictions. A predictive 3D model is thus crucial for obtaining a deeper understanding of RCF crack growth behaviour.

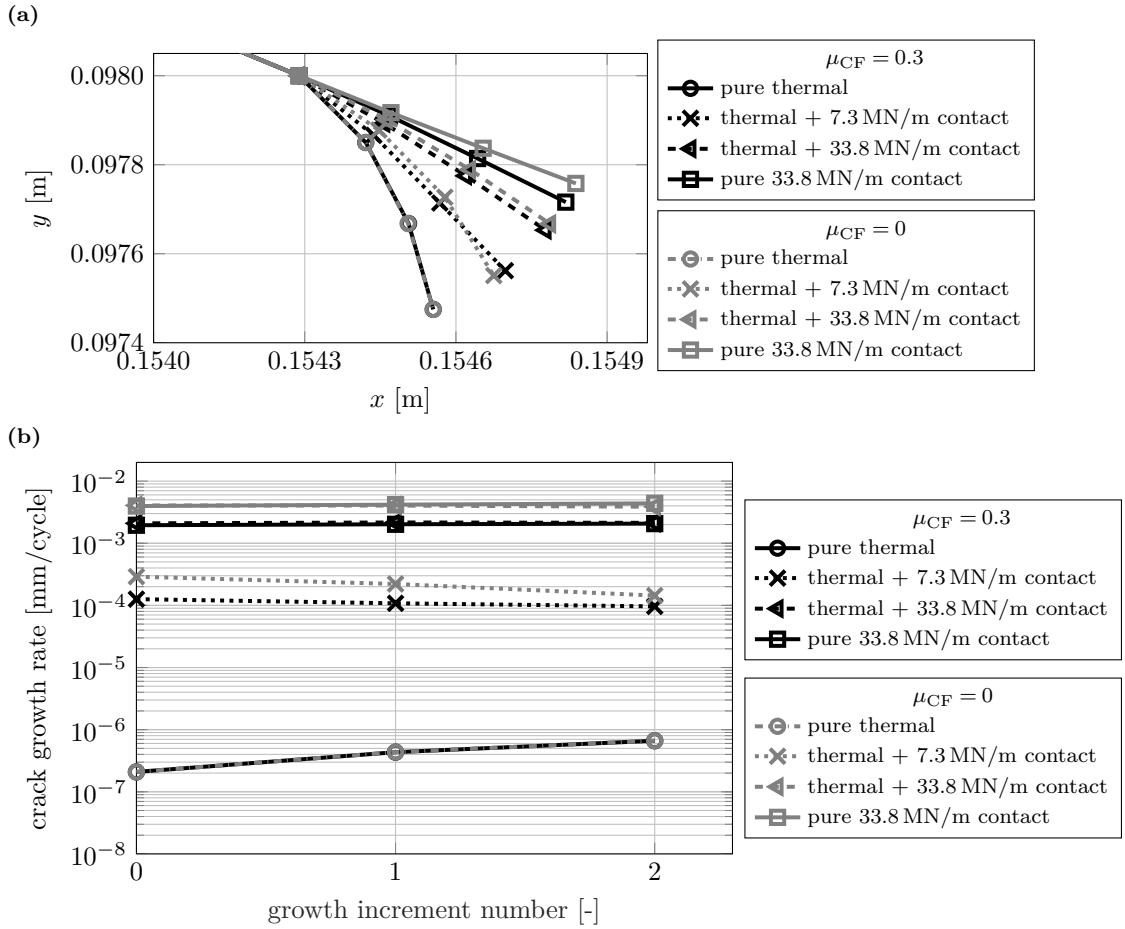

Figure 4.3: *Comparison of frictional ($\mu_{\mathrm{CF}} = 0.3$) and frictionless ($\mu_{\mathrm{CF}} = 0$) cracks under combined tensile thermal ($\Delta T = -20\,^{\circ}\mathrm{C}$) and contact loads with $f_{\mathrm{wr}} = 0.3$. (a) Predicted crack paths. (b) Upper estimates of predicted crack growth rates. Adapted from* ***Paper B****.*

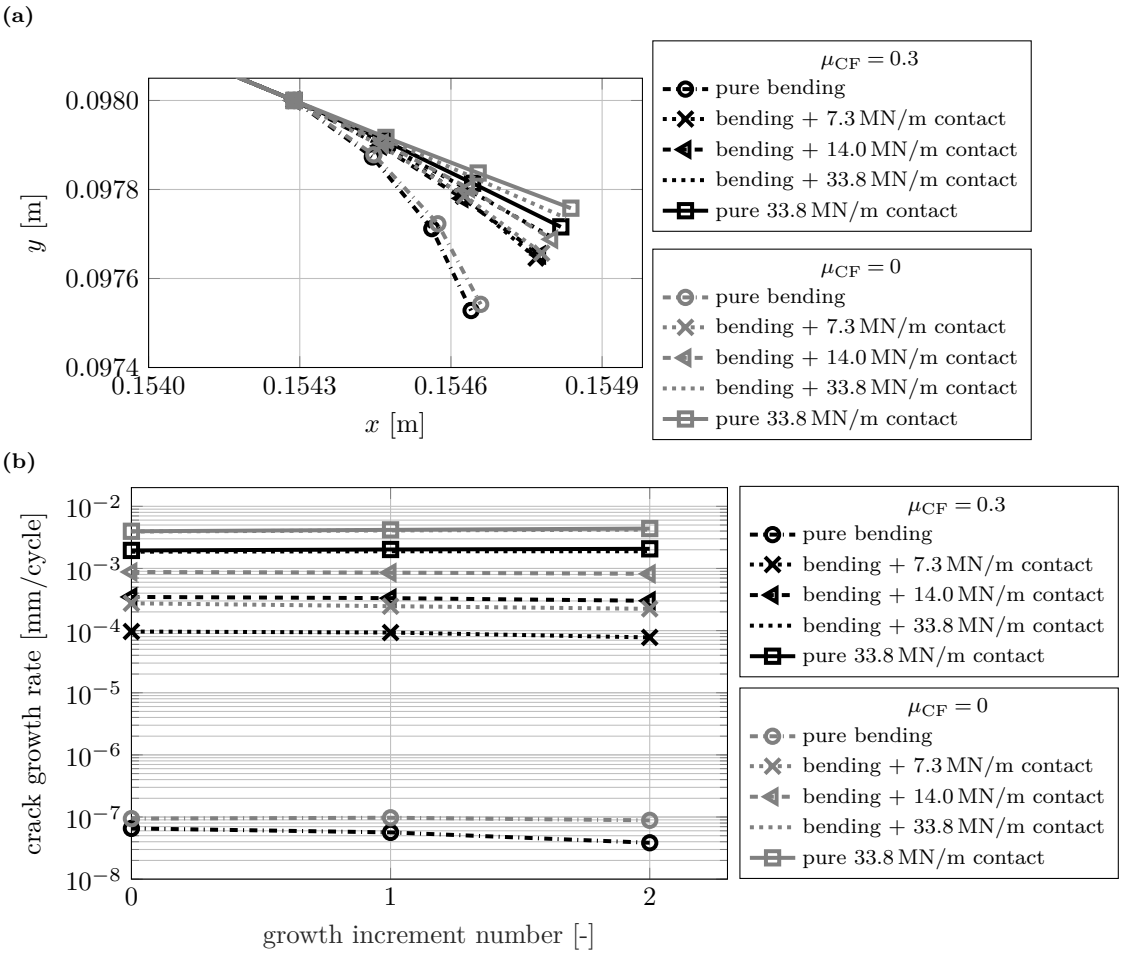

Figure 4.4: *Comparison of frictional ($\mu_{\mathrm{CF}} = 0.3$) and frictionless ($\mu_{\mathrm{CF}} = 0$) cracks under combined bending and contact loads with $f_{\mathrm{wr}} = 0.3$. (a) Predicted crack paths. (b) Upper estimates of predicted crack growth rates. Adapted from* ***Paper B****.*

4.4 Paper C: Finite element analyses of rail head cracks: Predicting direction and rate of rolling contact fatigue crack growth

The aim of this paper is to predict crack growth directions and rates in a 3D analysis. For this, the previously developed numerical framework in **Papers A** and **B** is first extended to 3D for a stationary crack to predict crack growth direction and rate in a rail head. An inclined semi-circular surface-breaking gauge corner crack with frictionless crack faces is incorporated into a 60E1 rail model (shown in Fig. 3.2), and the load scenarios of **Paper A** are studied. The crack growth direction is predicted using the modified accumulative VCTD criterion as proposed in **Paper B**, where the influence of modes I and II are considered on the predicted direction. The two Paris-type equations employed in **Paper B** are extended to take into account mode III effects on the estimated crack growth rates. The crack is stationary in this study and results are evaluated at three points along the crack front (shown in Fig. 3.3a) for four crack radii and two crack plane inclinations. The rate predictions were found to have a reasonable match with field measurements in the literature.

It is found that the crack is generally predicted to go deeper into the rail under the combined load cases and in the presence of tractive forces than under pure contact load, see Fig. 4.5. Crack growth rates for the combined load cases, as upper estimates shown in Fig. 4.6, are generally higher than (but still close to) those of pure contact load cases. Under the studied load magnitude, it is observed that a tractive force increases growth rates for smaller cracks, $r \leq 5\,\text{mm}$, whereas a steeper crack plane inclination ($\varphi = 45°$) decreases the growth rate as compared to a shallower inclination ($\varphi = 25°$).

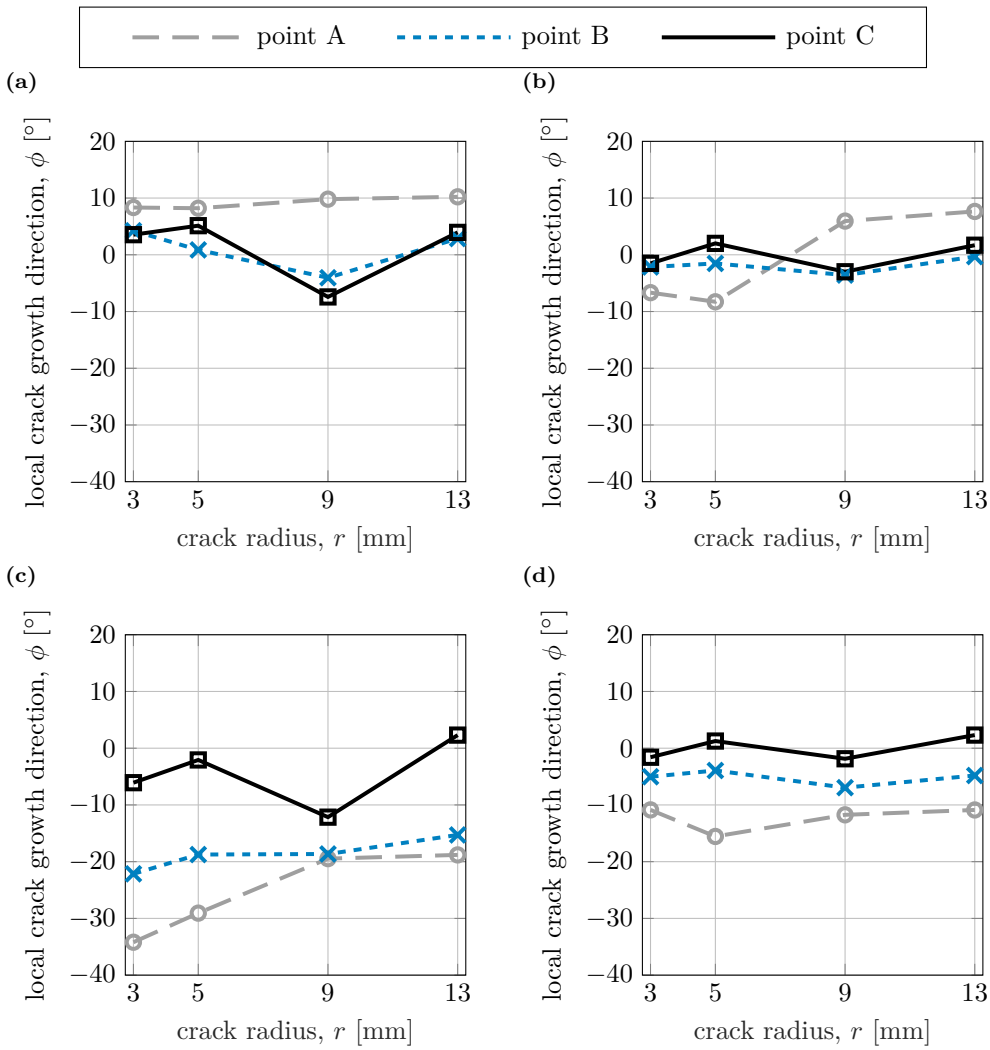

Figure 4.5: *Predicted growth directions, crack plane inclination of* $\varphi = 25°$. *(a) Pure contact,* 7.5 t *wheel load,* $f_{\mathrm{wr}} = 0$. *(b) Pure contact,* 7.5 t *wheel load,* $f_{\mathrm{wr}} = 0.3$. *(c) Tensile thermal* ($\Delta T = -20\,°\mathrm{C}$) *and* 7.5 t *wheel load,* $f_{\mathrm{wr}} = 0.3$. *(d) Bending and* 7.5 t *wheel load,* $f_{\mathrm{wr}} = 0.3$. *From* ***Paper C****.*

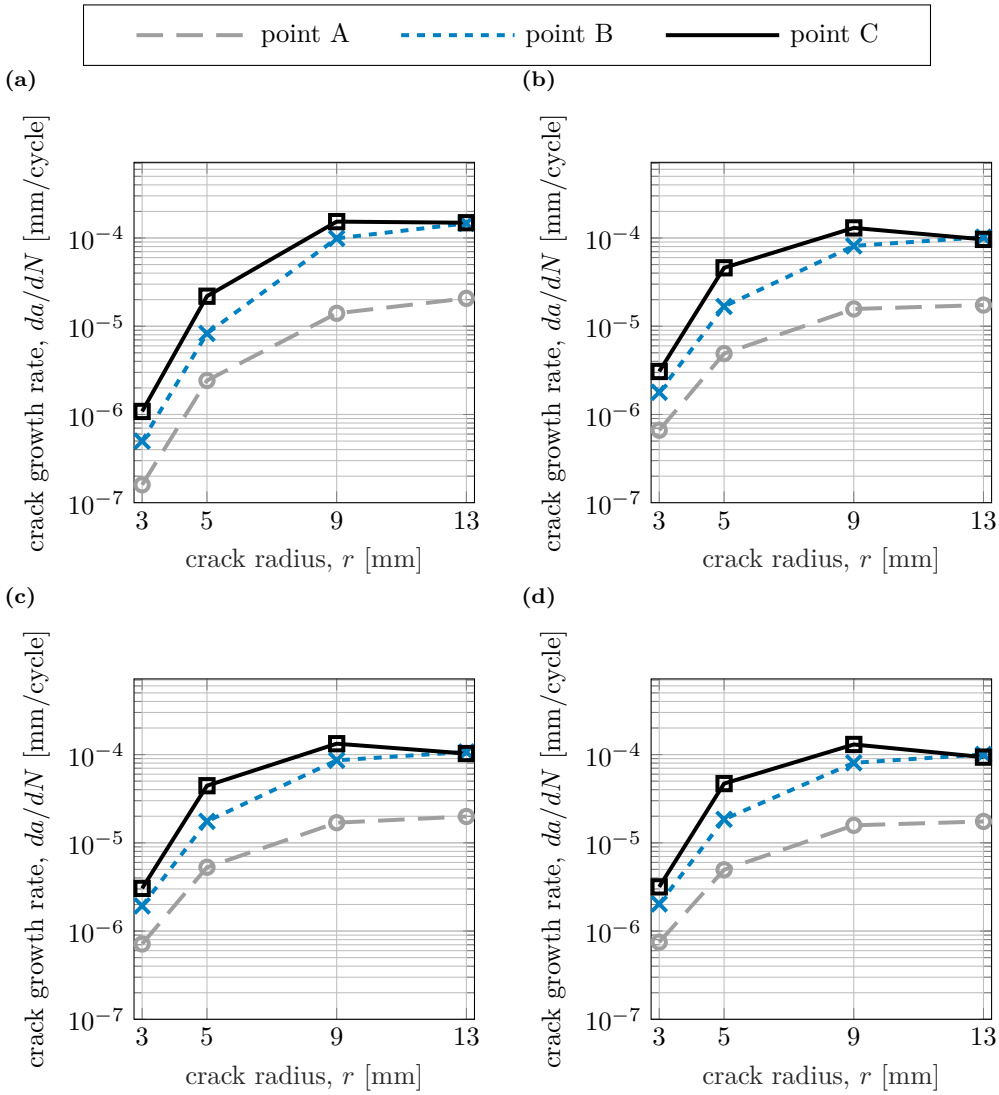

Figure 4.6: *Upper estimate of predicted growth rates, crack plane inclination of* $\varphi = 25°$. *(a) Pure contact,* 7.5 t *wheel load,* $f_{\mathrm{wr}} = 0$. *(b) Pure contact,* 7.5 t *wheel load,* $f_{\mathrm{wr}} = 0.3$. *(c) Tensile thermal* ($\Delta T = -20\,°\mathrm{C}$) *and* 7.5 t *wheel load,* $f_{\mathrm{wr}} = 0.3$. *(d) Bending and* 7.5 t *wheel load,* $f_{\mathrm{wr}} = 0.3$. *Adapted from* ***Paper C****.*

4.5 Paper D: Rolling contact fatigue crack propagation in rails – numerical investigation on consequences of operational load variations

This paper focuses on performing a parametric study on the influence of varying operational loads on predicted crack growth directions and rates using the numerical framework developed in **Paper C**. For the parametric study, the crack plane inclination is fixed to $\varphi = 25°$. Two different track support conditions ('nominal' and 'poor' as defined in **Paper D**), and two different thermal loads are employed in combination with wheel–rail contact load of different magnitudes and positions. This study highlights the sensitivities and limitations of the developed framework in **Paper C** and provides better conclusions regarding the influence of the considered load scenarios. In addition, rail lives under different load scenarios are estimated, which can be of use in maintenance planning.

It is observed that the ratio between the contact load and thermal/bending load is influential for crack growth direction under combined load cases. As shown in Figs. 4.7a and 4.8a, increasing the thermal load, or having 'poor' track support conditions while keeping the contact load constant, promotes downwards growth while increasing the wheel load magnitude in the presence of constant bending or thermal load leads to shallower growth directions. A shallower crack growth can also be obtained by moving a contact load towards the crack center. Crack growth rates for the combined load cases (upper estimates shown in Figs. 4.7b and 4.8b) are generally higher than (but still close to) those of the corresponding pure contact load cases with slightly higher values for the increased thermal or 'poor' track support conditions case. Also, the contact load magnitude and position mainly influence the crack growth rate.

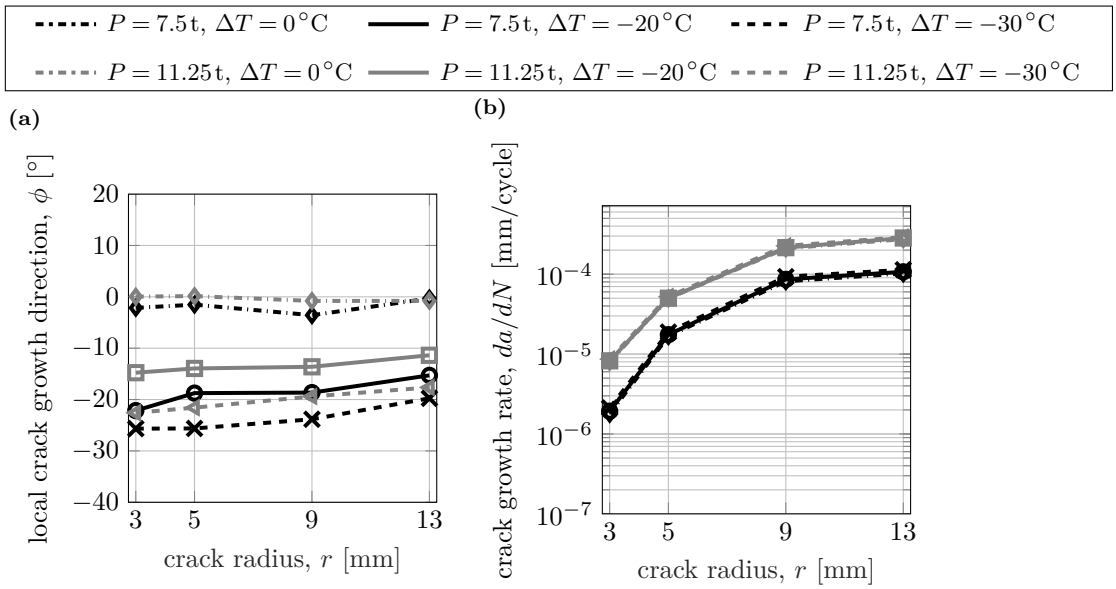

Figure 4.7: *Predicted crack growth at point B under combined tensile thermal and wheel load P with $f_{\mathrm{wr}} = 0.3$. (a) Predicted crack growth directions. (b) Upper estimates of predicted crack growth rates. From* ***Paper D****.*

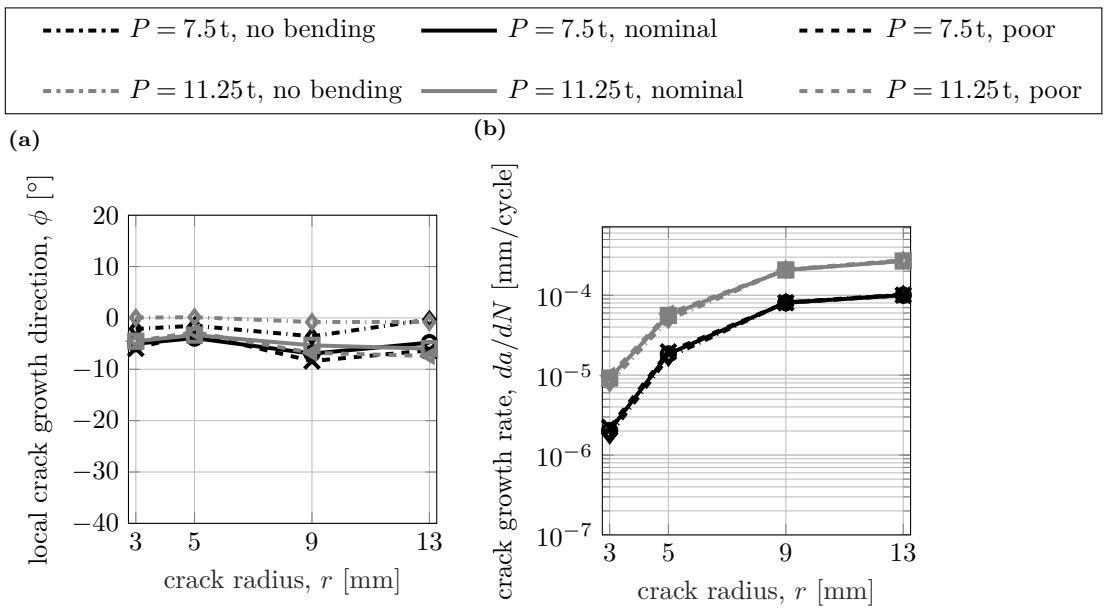

Figure 4.8: *Predicted crack growth at point B under combined bending with different track support conditions and wheel load P with $f_{\mathrm{wr}} = 0.3$. (a) Predicted crack growth directions. (b) Upper estimates of predicted crack growth rates. From* ***Paper D****.*

5 Concluding remarks and future work

5.1 Main results

This research deals with the influence of operational loading conditions on RCF crack propagation. For this, a numerically robust framework setting out from criteria and methods in the literature (and fine-tuning them when needed) has been developed for an unbiased propagating crack in a 2D model and a stationary crack in a 3D model (research objective 1 in Section 1.2). From the conducted study, the following conclusions can be drawn (research objectives 2 and 3 in Section 1.2):

- The predicted crack path for a frictionless crack under combined thermal and contact loads is found to change gradually from transverse growth (corresponding to pure thermal loading) to shallow growth (corresponding to a pure contact load), while there is an abrupt variation in the predicted crack path under combined bending and contact loads as the contact load is increased (**Paper A**).
- Predicted crack paths under pure contact load and under combined bending and contact loads are found to be moderately sensitive to the employed value of the reversed shear threshold parameter, ψ (**Paper A**).
- Two modifications of the crack growth direction criterion are investigated. A change in mid-value calculations under thermal and contact load is proposed. Further, the reversed shear condition is abandoned since it can yield unphysical predictions under the investigated combined loads for a frictional crack. Removing the condition also makes the predictions (slightly) better match the results from a twin-disc experiment (**Paper B**).
- A frictional crack tends to grow deeper into the rail than its frictionless counterpart under pure contact load and combinations of bending and contact loads (**Paper B**).
- Crack face friction has a moderate influence on predicted crack paths under combined thermal and contact loads (**Paper B**).
- Crack face friction reduces the crack growth rate in all investigated cases (**Paper B**).
- The predicted final growth direction is almost insensitive to the size of the growth increment in the numerical procedure. The growth direction typically converges towards the final direction after a few load cycles (**Papers A** and **B**).
- A crack under pure contact load without tractive forces tends to grow upwards. Adding a tractive force promotes downward growth and increases the crack growth rate for smaller crack sizes. Superposing a tensile thermal or bending loading also

increases the downward growth tendency and crack growth rate (**Papers C** and **D**).

- For the assumed semi-circular crack, the gauge side part of the crack deviates the most from the initial crack inclination with the slowest crack growth rate. The center side of the crack has the least deviation from the initial crack inclination (**Papers C** and **D**).
- A steeper crack plane inclination reduces the growth rate and introduces more fluctuations in the predicted growth directions (**Paper C**).
- An increased thermal load, or having 'poor' track support conditions while keeping the contact load constant, increases the growth rate and the tendency for downward growth (**Paper D**).
- Moving the contact load position towards the gauge side increases the crack growth rate without changing the trend of predicted growth directions but with slightly shallower directions (**Paper D**).
- Higher wheel load magnitudes increase the crack growth rate, and result in shallower crack growth (**Paper D**).
- Influence of longitudinal traction drops (substantially) with crack depth (**Papers C** and **D**).
- For the assumed semi-circular crack, longitudinal loads in combined load cases have the most influence in the point on the gauge side and the least influence in the point on center side (**Papers C** and **D**).
- Rail life reduces under combined load cases as compared to the pure contact load case (**Paper D**).

Table 5.1 summarizes the influence of investigated parameters.

5.2 Implications for railway operations

There are several practical implications related to this research (research objective 4 in Section 1.2). Some of these are:

- The wheel–rail contact load has a major influence on the predictions of the crack growth direction and rate (**Papers A**–**D**).
- As a tensile thermal load increases downward growth propensity and growth rate, it is recommended to perform inspections before/at the beginning of the winter season and to have shorter inspection intervals as long as these conditions prevail (**Papers A**–**D**).

Table 5.1: The resulting outcomes of the considered parameter variations (C: contact, B: bending, T: tensile thermal).

loading	parameter	crack growth rate	crack growth direction
C	wheel–rail traction	↑ for smaller cracks	deeper
	wheel load magnitude	↑ for higher C	shallower for ↑ C
	contact load position	↑ for C closer to crack	shallower for C closer to crack
	steeper crack plane inclination	↓	more fluctuations
	crack face friction	↓	deeper
B+C	compared to C with traction	↑	deeper
	'poor' track support conditions	↑	deeper
	wheel load magnitude	↑ for higher C	shallower for ↑ C
	contact load position	↑ for C closer to crack	shallower for C closer to crack
	steeper crack plane inclination	↓	more fluctuations
	crack face friction	↓	deeper
T+C	compared to C with traction	↑	deeper
	thermal load magnitude	↑ for higher T	deeper for ↑ T
	wheel load magnitude	↑ for higher C	shallower for ↑ C
	contact load position	↑ for C closer to crack	shallower for C closer to crack
	steeper crack plane inclination	↓	more fluctuations
	crack face friction	↓	moderate influence

- Crack face friction typically promotes more downward growth and reduces crack growth rate. The former is detrimental while the latter is beneficial from a maintenance planning perspective (**Paper B**).
- Longitudinal tractive forces are detrimental for the growth of smaller cracks, i.e., close to the rail surface, as they promote downward growth with an increase in growth rate. However, this effect drops (significantly) with depth (**Papers C** and **D**).
- Assuming the same conditions in ambient temperature and track support conditions, increasing the allowed axle load of a line would increase the crack growth rate. However, it will promote shallower crack growth (**Paper D**).
- Track support conditions are important as a 'poor' (i.e., soft) condition leads to more downward crack growth with higher rates (**Paper D**).
- The distance between the wheel–rail contact point and the crack location has a high influence on crack growth rates (**Paper D**).
- Cracks with steeper plane inclination exhibit more fluctuations in growth directions and lower crack growth rates (**Paper C**). However, the detection of these cracks in rails is more difficult due to larger shielding effects [84].
- The gauge side of the crack front is more influenced by the longitudinal bending and tensile thermal loads while the influence is reduced for the center side of the

crack front (**Papers C** and **D**).

- For smaller cracks, the gauge side part of the crack tends to grow downwards with the slowest crack growth rate. The center side of the crack grows shallowly into the rail with a faster crack growth rate (**Papers C** and **D**).

5.3 Open questions

Several open questions regarding RCF crack propagation remain. Some of these are:

- Crack advancement modelling and incorporating crack face friction would improve 3D predictions and make validations against experimental/field data possible. For considering a propagating crack, the numerical efficiency of the framework needs to be improved, and a suitable description of the evolving crack geometry must be adopted.
- The current study qualitatively compared the influence of the operational loading conditions. Further calibrations need to be considered for more precise quantitative comparisons.
- For gauge corner cracking, wear would also be of importance for quantitative (growth rate) predictions. This can be incorporated into the numerical framework. Moreover, the contact formulation has a direct influence on the predictions. In future calibrations, the contact load formulation may need to change to non-Hertzian (some of these models have been mentioned in Section 2.4), and lateral tangential contact forces may need to be accounted for.
- Investigating the influence of the material anisotropy and inelasticity that exists in a layer close to the rail surface on the growth of surface-breaking cracks will increase the understanding of the crack growth behaviour. This can be done by considering a proper elastic-plastic material model and developing a more generally applicable crack growth criteria if needed. Considering the inelasticity of the rail material also allows for over-rolling simulations to study the influence of multiple wheel passages on crack growth.
- The thesis considers the growth of an individual crack in a rail head. For simulating interaction between cracks similar to crack networks typically seen in the field, model extensions would be needed.

References

[1] *SIKA Basfakta 2008 – Övergripande statistik om transportsektorn, 2009:28 (in Swedish)*. Statens institut för kommunikationsanalys (SIKA), 2009, 125 p.

[2] *The future of rail: Opportunities for energy and the environment*. International Energy Agency (IEA), Paris, 2019, 175 p.

[3] K. L. Johnson. The strength of surfaces in rolling contact. *Proceedings of the Institution of Mechanical Engineers, Part C: Mechanical Engineering Science* 203.3 (1989), 151–163.

[4] C. Doll, C. Brauer, J. Köhler, and P. Scholten. *Methodology for GHG efficiency of transport modes*. Fraunhofer-Institute for Systems and Innovation Research ISI, 2020, 88 p.

[5] H. Hertz. Ueber die berührung fester elastischer körper (in German). *Journal für die reine und angewandte Mathematik* 92 (1882), 156–171.

[6] M. B. Marshall, R. Lewis, R. S. Dwyer-Joyce, U. Olofsson, and S. Björklund. Experimental characterization of wheel-rail contact patch evolution. *Journal of Tribology* 128.3 (2006), 493–504.

[7] E. E. Magel. *Rolling contact fatigue: A comprehensive review*. US Department of Transportation, Federal Railroad Administration, 2011, 132 p.

[8] D. F. Cannon, K.-O. Edel, S. L. Grassie, and K. Sawley. Rail defects: an overview. *Fatigue & Fracture of Engineering Materials & Structures* 26.10 (2003), 865–886.

[9] A. Ekberg and E. Kabo. Fatigue of railway wheels and rails under rolling contact and thermal loading – an overview. *Wear* 258.7–8 (2005), 1288–1300.

[10] R. Dollevoet. *Design of an anti head check profile based on stress relief*. PhD thesis. University of Twente, 2010, 151 p.

[11] *IRS 70712: Rail defects*. International Union of Railways (UIC), 1st edition, 2018-5, 2018, 115 p.

[12] J. W. Ringsberg. Life prediction of rolling contact fatigue crack initiation. *International Journal of Fatigue* 23.7 (2001), 575–586.

[13] N. Talebi, J. Ahlström, M. Ekh, and K. A. Meyer. Evaluations and enhancements of fatigue crack initiation criteria for steels subjected to large shear deformations. *International Journal of Fatigue* 182 (2024), 108227.

[14] G. R. Irwin. Analysis of stresses and strains near the end of a crack traversing a plate. *Journal of Applied Mechanics* 24.3 (1957), 361–364.

[15] Y. Murakami. *Stress intensity factors handbook, Volume I*. Pergamon, 1987, 640 p.

[16] Y. Murakami. *Stress intensity factors handbook, Volume II*. Pergamon, 1987, 816 p.

[17] Y. Murakami. *Stress intensity factors handbook, Volume III*. Pergamon, 1992, 1062 p.

[18] M. Kuna. *Finite elements in fracture mechanics: Theory - Numerics - Applications*. Springer Netherlands, 2013, 447 p.

[19] N. K. Mukhopadhyay, S. K. Maiti, and A. Kakodkar. A review of SIF evaluation and modelling of singularities in BEM. *Computational Mechanics* 25.4 (2000), 358–375.

[20] S. N. Atluri (ed.). *Computational methods in the mechanics of fracture*. Elsevier Science Publishers B.V., Amsterdam, 1986, 414 p.

[21] G. Cherepanov. Crack propagation in continuous media. *Journal of Applied Mathematics and Mechanics* 31.3 (1967), 503–512.

[22] J. R. Rice. A path independent integral and the approximate analysis of strain concentration by notches and cracks. *Journal of Applied Mechanics* 35.2 (1968), 379–386.

[23] C. T. Sun and Z.-H. Jin. *Fracture mechanics*. Academic Press, 2012, 311 p.

[24] R. Andersson, F. Larsson, and E. Kabo. Evaluation of stress intensity factors under multiaxial and compressive conditions using low order displacement or stress field fitting. *Engineering Fracture Mechanics* 189 (2018), 204–220.

[25] D. Ngo and A. Scordelis. Finite element analysis of reinforced concrete beams. *ACI Journal Proceedings* 64.3 (1967), 152–163.

[26] R. D. Henshell and K. G. Shaw. Crack tip finite elements are unnecessary. *International Journal for Numerical Methods in Engineering* 9.3 (1975), 495–507.

[27] R. S. Barsoum. On the use of isoparametric finite elements in linear fracture mechanics. *International Journal for Numerical Methods in Engineering* 10.1 (1976), 25–37.

[28] R. Branco, F. Antunes, and J. Costa. A review on 3D-FE adaptive remeshing techniques for crack growth modelling. *Engineering Fracture Mechanics* 141 (2015), 170–195.

[29] T. Belytschko and T. Black. Elastic crack growth in finite elements with minimal remeshing. *International Journal for Numerical Methods in Engineering* 45.5 (1999), 601–620.

[30] N. Moës, J. Dolbow, and T. Belytschko. A finite element method for crack growth without remeshing. *International Journal for Numerical Methods in Engineering* 46.1 (1999), 131–150.

[31] A. R. Khoei. *Extended finite element method: Theory and applications*. John Wiley Sons, Ltd, 2014, 565 p.

[32] P. Wriggers. *Computational contact mechanics*. Springer Berlin Heidelberg, 2006, 518 p.

[33] N. E. Dowling. *Mechanical behavior of materials: engineering methods for deformation, fracture, and fatigue*. Pearson Education, 2012, 954 p.

[34] P. Paris and F. Erdogan. A critical analysis of crack propagation laws. *Journal of Basic Engineering* 85.4 (1963), 528–533.

[35] F. Erdogan and G. C. Sih. On the crack extension in plates under plane loading and transverse shear. *Journal of Basic Engineering* 85.4 (1963), 519–525.

[36] P. Dahlin and M. Olsson. The effect of plasticity on incipient mixed-mode fatigue crack growth. *Fatigue & Fracture of Engineering Materials & Structures* 26.7 (2003), 577–588.

[37] A. Abdel Mageed and R. Pandey. Fatigue crack closure in kinked cracks and path of crack propagation. *International Journal of Fracture* 44.1 (1990), 39–42.

[38] M. Schöllmann, H. A. Richard, G. Kullmer, and M. Fulland. A new criterion for the prediction of crack development in multiaxially loaded structures. *International Journal of Fracture* 117.2 (2002), 129–141.

[39] S. Biner. Fatigue crack growth studies under mixed-mode loading. *International Journal of Fatigue* 23. Supplement 1 (2001), 259–263.

[40] A. Abdel Mageed and R. Pandey. Mixed mode crack growth under static and cyclic loading in Al-alloy sheets. *Engineering Fracture Mechanics* 40.2 (1991), 371–385.

[41] A. Abdel Mageed and R. Pandey. Studies on cyclic crack path and the mixed-mode crack closure behaviour in Al alloy. *International Journal of Fatigue* 14.1 (1992), 21–29.

[42] P. E. Bold, M. W. Brown, and R. J. Allen. Shear mode crack growth and rolling contact fatigue. *Wear* 144.1 (1991), 307–317.

[43] D. Floros, A. Ekberg, and F. Larsson. Evaluation of crack growth direction criteria on mixed-mode fatigue crack growth experiments. *International Journal of Fatigue* 129 (2019), 105075.

[44] K. Tanaka. Fatigue crack propagation from a crack inclined to the cyclic tensile axis. *Engineering Fracture Mechanics* 6.3 (1974), 493–507.

[45] Y. Xiangqiao, D. Shanyi, and Z. Zehua. Mixed-mode fatigue crack growth prediction in biaxially stretched sheets. *Engineering Fracture Mechanics* 43.3 (1992), 471–475.

[46] S. Bogdaski, J. Stupnicki, M. W. Brown, and D. F. Cannon. A two dimensional analysis of mixed-mode rolling contact fatigue crack growth in rails. *European Structural Integrity Society* 25 (1999), 235–248.

[47] J. Qian and A. Fatemi. Mixed mode fatigue crack growth: A literature survey. *Engineering Fracture Mechanics* 55.6 (1996), 969–990.

[48] H. Richard, B. Schramm, and N.-H. Schirmeisen. Cracks on mixed mode loading - Theories, experiments, simulations. *International Journal of Fatigue* 62 (2014), 93–103.

[49] G. R. Irwin. Fracture strength relative to onset and arrest of crack propagation. *Proceedings of ASTM* 58 (1958), 640–657.

[50] N. E. Dowling and J. A. Begley. Fatigue crack growth during gross plasticity and the J-Integral. *ASTM special technical publications* (1976), 82–103.

[51] T. Hoshide and D. Socie. Mechanics of mixed mode small fatigue crack growth. *Engineering Fracture Mechanics* 26.6 (1987), 841–850.

[52] D. M. Parks. A stiffness derivative finite element technique for determination of crack tip stress intensity factors. *International Journal of Fracture* 10 (1974), 487–502.

[53] T. K. Hellen. On the method of virtual crack extensions. *International Journal for Numerical Methods in Engineering* 9.1 (1975), 187–207.

[54] G. C. Sih. Strain-energy-density factor applied to mixed mode crack problems. *International Journal of Fracture* 10.3 (1974), 305–321.

[55] G. C. Sih. *Mechanics of fracture initiation and propagation.* Springer Netherlands, 1991, 410 p.

[56] G. A. Maugin. Material forces: concepts and applications. *Applied Mechanics Reviews* 48.5 (1995), 213–245.

[57] M. E. Gurtin and P. Podio-Guidugli. Configurational forces and a constitutive theory for crack propagation that allows for kinking and curving. *Journal of the Mechanics and Physics of Solids* 46.8 (1998), 1343–1378.

[58] J. Brouzoulis and M. Ekh. Crack propagation in rails under rolling contact fatigue loading conditions based on material forces. *International Journal of Fatigue* 45 (2012), 98–105.

[59] D. Floros, F. Larsson, and K. Runesson. On configurational forces for gradient-enhanced inelasticity. *Computational Mechanics* 61 (2018), 409–432.

[60] A. A. Wells. Critical tip opening displacement as fracture criterion. *Proceedings of Crack Propagation Symposium, Cranfield* (1961), 210–221.

[61] D. Rozumek and E. Macha. A survey of failure criteria and parameters in mixed-mode fatigue crack growth. *Materials Science* 45.2 (2009), 190–210.

[62] C. Li. Vector CTD criterion applied to mixed mode fatigue crack growth. *Fatigue & Fracture of Engineering Materials & Structures* 12.1 (1989), 59–65.

[63] D. Floros. *Finite element procedures for crack path prediction in multi-axial fatigue.* PhD thesis. Chalmers University of Technology, 2018, 146 p.

[64] F. Hourlier and A. Pineau. Propagation of fatigue cracks under polymodal loading. *Fatigue & Fracture of Engineering Materials & Structures* 5.4 (1982), 287–302.

[65] F. Hourlier, H. d'Hondt, M. Truchon, and A. Pineau. Fatigue crack path behavior under polymodal fatigue. *Multiaxial Fatigue. ASTM International* (1985), 228–248.

[66] P. E. Bold, M. W. Brown, and R. J. Allen. A review of fatigue crack growth in steels under mixed mode I and II loading. *Fatigue & Fracture of Engineering Materials & Structures* 15.10 (1992), 965–977.

[67] P. Zerres and M. Vormwald. Review of fatigue crack growth under non-proportional mixed-mode loading. *International Journal of Fatigue* 58 (2014), 75–83.

[68] A. Ekberg and E. Kabo. *Surface fatigue initiated transverse defects and broken rails – an International Review.* 2014, 24 p.

[69] D. Floros, A. Ekberg, and F. Larsson. Evaluation of mixed-mode crack growth direction criteria under rolling contact conditions. *Wear* 448-449 (2020), 203184.

[70] K. L. Johnson. *Contact mechanics.* Cambridge University Press, 1985.

[71] J. J. Kalker. *Three-dimensional elastic bodies in rolling contact.* Springer Dordrecht, 1990, 314 p.

[72] S. Timoshenko and J. N. Goodier. *Theory of elasticity.* McGraw-Hill, 1951, 506 p.

[73] R. Skrypnyk, J. C. O. Nielsen, M. Ekh, and B. A. Pålsson. Metamodelling of wheel-rail normal contact in railway crossings with elasto-plastic material behaviour. *Engineering with Computers* 35.1 (2019), 139–155.

[74] Z. Li. *Wheel-rail rolling contact and its application to wear simulation.* PhD thesis. Delft University of Technology, 2002, 166 p.

[75] J. B. Ayasse and H. Chollet. Determination of the wheel rail contact patch in semi-Hertzian conditions. *Vehicle System Dynamics* 43.3 (2005), 161–172.

[76] X. Quost, M. Sebes, A. Eddhahak, J. B. Ayasse, H. Chollet, P. E. Gautier, and F. Thouverez. Assessment of a semi-Hertzian method for determination of wheelrail contact patch. *Vehicle System Dynamics* 44.10 (2006), 789–814.

[77] J. J. Kalker. The principle of virtual work and its dual for contact problems. *Ingenieur-Archiv* 56 (1986), 453–467.

[78] S. Z. Meymand, A. Keylin, and M. Ahmadian. A survey of wheel-rail contact models for rail vehicles. *Vehicle System Dynamics* 54.3 (2016), 386–428.

[79] *CEN. Railway applications - track - rail - Part 1: vignole railway rails 46 kg/m and above. EN 13674-1:2011.* Europeean Committee for Standardization, 2011.

[80] J. C. O. Nielsen and A. Igeland. Vertical dynamic interaction between train and track influence of wheel and track imperfections. *Journal of Sound and Vibration* 187.5 (1995), 825–839.

[81] E. Lansler and E. Kabo. Subsurface crack face displacements in railway wheels. *Wear* 258.7-8 (2005), 1038–1047.

[82] *ABAQUS/Standard user's manual, version 2020.* Dassault Systèmes Simulia Corp., 2020.

[83] *MATLAB 9.7.0.1190202 (R2019b).* The MathWorks Inc., 2019.

[84] E. Magel, P. Mutton, A. Ekberg, and A. Kapoor. Rolling contact fatigue, wear and broken rail derailments. *Wear* 366–367 (2016), 249–257.